Efimov States in Nuclear and Particle Physics

Hans-Werner Hammer[1] and Lucas Platter[2,3]

[1]Helmholtz-Institut für Strahlen- und Kernphysik (Theorie) and Bethe Center for Theoretical Physics, Universität Bonn, 53115 Bonn, Germany; email: hammer@hiskp.uni-bonn.de

[2]Institute for Nuclear Theory, University of Washington, Seattle, Washington 98195; email: lplatter@phys.washington.edu

[3]Department of Physics, The Ohio State University, Columbus, Ohio 43210

Annu. Rev. Nucl. Part. Sci. 2010. 60:207–36

The *Annual Review of Nuclear and Particle Science* is online at nucl.annualreviews.org

This article's doi: 10.1146/annurev.nucl.012809.104439

0163-8998/10/1123-0207$20.00

Key Words

universality, Efimov physics, few-body systems, discrete scale invariance, hyperspherical formalism, effective field theory

Abstract

Particles with resonant short-range interactions have universal properties that do not depend on the details of their structure or their interactions at short distances. In the three-body system, these properties include the existence of a geometric spectrum of three-body Efimov states and a discrete scaling symmetry, which leads to log-periodic dependence of observables on the scattering length. Similar universal properties appear in the four-body system and possibly higher-body systems as well. For example, universal four-body states have recently been predicted and observed in experiments. These phenomena are often referred to as Efimov physics. We review their theoretical description and discuss applications in different areas of physics with a special emphasis on nuclear and particle physics.

Contents

1. INTRODUCTION

The scattering of particles with sufficiently low kinetic energy is determined by the particles' S-wave scattering length a, assuming that their de Broglie wavelengths are large compared with the range of the interaction. Generically, the scattering length a is comparable in magnitude to the range ℓ of the interaction: $|a| \sim \ell$. In exceptional cases, the scattering length can be much larger in magnitude than the range: $|a| \gg \ell$. Such a large scattering length requires the fine-tuning of a parameter characterizing the interactions to the neighborhood of a critical value at which a diverges to $\pm\infty$. If the scattering length is large, the particles exhibit properties that depend on a but are insensitive to the range and other details of the short-range interaction. These properties are universal: They apply equally well to any nonrelativistic particle with short-range interactions that produce a large scattering length (1, 2).

For example, in the case of equal-mass particles with mass m and $a > 0$, there is a two-body bound state near the scattering threshold with binding energy $B_d = \hbar^2/(ma^2)$. The corrections to this formula are suppressed by powers of ℓ/a. This bound state corresponds to a pole of the two-particle scattering amplitude at $E = -B_d$. If the scattering length is negative, there is a universal virtual state that corresponds to a pole on the unphysical second sheet in the complex energy plane.

The key evidence for universal behavior in the three-body system was the discovery of the Efimov effect in 1970 (3). In the unitary limit $1/a \to 0$, the two-body bound state is exactly at the two-body scattering threshold $E = 0$. Efimov showed that in this limit there are infinitely many arbitrarily shallow three-body bound states whose binding energies $B_t^{(n)}$ have an accumulation point at $E = 0$. The Efimov effect is only one aspect of universal properties in the three-body system. It has universal properties not only in the unitary limit but whenever the scattering length is large compared with the range ℓ. The universal properties include a discrete scaling symmetry. We refer to universal aspects associated with this discrete scaling symmetry as Efimov physics.

Although they are well established theoretically, Efimov states are difficult to precisely identify in nature because (*a*) typical systems are not in the unitary limit and (*b*) the scattering length cannot be varied. Perhaps the simplest example in nuclear physics is the triton. The triton can be

interpreted as the ground state of an Efimov spectrum in the *pnn* system with total spin $J = 1/2$. Because the ratio ℓ/a is only approximately 1/3, the whole spectrum contains only one state, but the low-energy properties of the triton can be described in this scenario. A promising system for observing several Efimov states is ^{4}He atoms, which have a scattering length that is more than a factor of ten larger than the range of the interaction. Calculations that use accurate potential models indicate that a system of three ^{4}He atoms has two three-body bound states or trimers. The ground-state trimer can be interpreted as an Efimov state, and it has been observed in experiments involving the scattering of cold jets of ^{4}He atoms from a diffraction grating (4). The excited trimer is universally believed to be an Efimov state, but it has not yet been observed.

The rapid development of the field of cold atom physics has opened up new opportunities for the experimental study of Efimov physics. These opportunities have been made possible by two separate technological developments. One is the technology for cooling atoms to the extremely low temperatures at which Efimov physics plays a crucial role. The other is the technology for controlling the interactions between atoms. By tuning the magnetic field to a Feshbach resonance, the scattering lengths of the atoms can be controlled experimentally and made arbitrarily large. Both developments were crucial in recent experiments that provided the first indirect evidence for the existence of Efimov states in ultracold atoms (5).

Overviews of Efimov physics in ultracold atomic gases can be found elsewhere (1, 2, 6). In this review, we focus on universal aspects and Efimov states in nuclear and particle physics. Even though the scattering length cannot be varied, there are many systems close to the unitary limit at which Efimov physics is relevant. They include few-nucleon systems, halo nuclei, and weakly bound hadronic molecules. These systems can be described in a universal effective field theory (EFT) that implements an expansion around the unitary limit. Three-body bound states can be interpreted as Efimov trimers.

In the next section, we review the physics of the Efimov effect, beginning with a brief account of the history. In the following sections, we discuss applications in nuclear and particle physics. We end with a summary and outlook.

2. PHYSICS OF THE EFIMOV EFFECT

2.1. History

The first hints on universal behavior in the three-body system came from the 1935 discovery of the Thomas collapse (7), which is closely related to the Efimov effect. Thomas (7) studied the zero-range limit for potentials with a single two-body bound state with fixed energy. Using a variational argument, he showed that the binding energy $B_t^{(0)}$ of the deepest three-body bound state diverges to infinity in this limit. Thus, the spectrum of three-body bound states is unbounded from below.

Further progress was made through the application of the zero-range limit to the three-nucleon system. An integral equation for S-wave neutron-deuteron scattering via zero-range interactions was derived in 1957 by Skorniakov & Ter-Martirosian (8). For the spin-quartet channel, this integral equation has no bound-state solutions and is well behaved. In the spin-doublet channel, however, it has solutions for arbitrary energy (9), including bound-state solutions. If the solution is fixed by requiring a specific three-body energy, the resulting equation still has a discrete spectrum that extends to minus infinity (10, 11), in agreement with the earlier result of Thomas. Although a prediction for the spin-doublet neutron-deuteron scattering length was obtained by use of the triton binding energy as input (12), most subsequent work focused on finite-range forces that avoid this pathology at high energies.

In 1970, Efimov (3) realized that one should focus on the physics at low energies, $E \ll \hbar^2/(m\ell^2)$, and not on the deepest states. In this limit, where zero-range forces are adequate, he arrived at some surprising results. He pointed out that when $|a|$ is sufficiently large compared with the range ℓ of the potential, there is a sequence of three-body bound states whose binding energies are spaced roughly geometrically in the interval between $\hbar^2/(m\ell^2)$ and $\hbar^2/(ma^2)$. As $|a|$ is increased, new bound states appear in the spectrum at critical values of a that differ by multiplicative factors of e^{π/s_0}, where s_0 depends on the statistics and the mass ratios of the particles. In the case of spin-doublet neutron-deuteron scattering and for three identical bosons, s_0 is the solution to the transcendental equation

$$s_0 \cosh \frac{\pi s_0}{2} = \frac{8}{\sqrt{3}} \sinh \frac{\pi s_0}{6}. \qquad 1.$$

Its numerical value is $s_0 \approx 1.00624$, so $e^{\pi/s_0} \approx 22.7$. As $|a|/\ell \to \infty$, the asymptotic number of three-body bound states is

$$N \to \frac{s_0}{\pi} \ln \frac{|a|}{\ell}. \qquad 2.$$

In the limit $a \to \pm\infty$, there are infinitely many three-body bound states with an accumulation point at the three-body scattering threshold with a geometric spectrum

$$B_t^{(n)} = (e^{-2\pi/s_0})^{n-n_*} \hbar^2 \kappa_*^2/m, \qquad 3.$$

where m is the mass of the particles and κ_* is the binding wave number of the branch of Efimov states labeled by n_*. The geometric spectrum in Equation 3 is the signature of a discrete scaling symmetry with scaling factor $e^{\pi/s_0} \approx 22.7$. It is independent of the mass or structure of the identical particles and independent of the form of their short-range interactions. The Efimov effect can also occur in other three-body systems if at least two of the three pairs have a large S-wave scattering length, but the numerical value of the asymptotic ratio may differ from 22.7.

A formal proof of the Efimov effect was subsequently given by Amado & Noble (13, 14). The Thomas and Efimov effects are closely related. The deepest three-body bound states found by Thomas's variational calculation can be identified with the deepest Efimov states (15). The mathematical connection of the Efimov effect to a limit cycle was discussed in Reference 16.

The universal properties in the three-body system with large scattering length are not restricted to the Efimov effect. The dependency of three-body observables on the scattering length or the energy is characterized by scaling-behavior modulo coefficients that are log-periodic functions of a (17, 18). This behavior is characteristic of a system with a discrete scaling symmetry.

In 1981, Efimov (19) proposed a new approach to the low-energy few-nucleon problem in nuclear physics that, in modern language, was based on perturbation theory around the unitary limit. Remarkably, this program works reasonably well in the three-nucleon system at momenta that are small compared with M_π. The Efimov effect requires that a boundary condition be imposed on the wave function at short distances. The boundary condition can be fixed by means of either the spin-doublet neutron-deuteron scattering length or the triton binding energy as input. If the deuteron binding energy is used as the two-body input and if the boundary condition is fixed by using the spin-doublet neutron-deuteron scattering length as input, the triton binding energy can be predicted with an accuracy of 6%. The accuracy of the predictions can be further improved by taking into account the effective range as a first-order perturbation (20). Thus, the triton can be identified as an Efimov state associated with the deuteron and the spin-singlet virtual state as a *pn* state with large scattering length (19).

In the three-nucleon system, this program was implemented within an EFT framework by Bedaque et al. (21–23). The authors (23) found that the renormalization of the EFT requires

a $SU(4)$-symmetric three-body interaction with an ultraviolet (UV) limit cycle. The three-body force depends on a parameter Λ_* that is determined through a renormalization condition that plays the same role as Efimov's boundary condition. $SU(4)$ symmetry was introduced in 1937 by Wigner (24) as a generalization of the $SU(2) \times SU(2)$ spin-isospin symmetry, allowing for a mixing of spin and isospin degrees of freedom in symmetry transformations. It is satisfied to a high degree in the energy spectra of atomic nuclei. Exact Wigner symmetry requires the S-wave scattering lengths in the spin-triplet and spin-singlet channels to be equal. However, if both two-body scattering lengths are large, it is a very good approximation even if they are different, because the symmetry-breaking terms are proportional to the inverse scattering lengths (25).

This EFT is ideally suited to calculating corrections to the universal results in the scaling limit. Its application to few-nucleon physics is discussed in Section 3.

2.2. Hyperspherical Methods

Coordinate-space methods are a valuable tool for the analysis of the three-body problem with short-range interactions (17, 26, 27). In this subsection, we introduce the hyperspherical approach that has been used to obtain important results about the Efimov spectrum. The material of this subsection is based on the discussion of the hyperradial formalism in Reference 1. For three particles of equal mass, the Jacobi coordinates are defined as

$$\mathbf{r}_{ij} = \mathbf{r}_i - \mathbf{r}_j \quad \text{and} \quad \mathbf{r}_{k,ij} = \mathbf{r}_k - \frac{1}{2}(\mathbf{r}_i + \mathbf{r}_j), \tag{4.}$$

where the triple (ijk) is a cyclic permutation of the particle indices (28). The hyperradius R and hyperangle α_k are then defined by

$$R^2 = \frac{1}{3}(\mathbf{r}_{12}^2 + \mathbf{r}_{23}^2 + \mathbf{r}_{31}^2) = \frac{1}{2}\mathbf{r}_{ij}^2 + \frac{2}{3}\mathbf{r}_{k,ij}^2 \quad \text{and} \quad \alpha_k = \arctan\left(\frac{\sqrt{3}|\mathbf{r}_{ij}|}{2|\mathbf{r}_{k,ij}|}\right), \tag{5.}$$

respectively. In the center-of-mass system, the Schrödinger equation in hyperspherical coordinates is given by

$$\left(T_R + T_{\alpha_k} + \frac{\Lambda_{k,ij}^2}{2mR^2} + V(R, \Omega)\right)\Psi(R, \alpha, \Omega) = E\Psi(R, \alpha, \Omega), \tag{6.}$$

where

$$T_R = \frac{\hbar^2}{2m} R^{-5/2}\left(-\frac{\partial}{\partial R^2} + \frac{15}{4R^2}\right) R^{5/2}, \tag{7.}$$

$$T_\alpha = \frac{\hbar^2}{2mR^2}\frac{1}{\sin 2\alpha}\left(-\frac{\partial^2}{\partial \alpha^2} - 4\right)\sin 2\alpha, \tag{8.}$$

and

$$\Lambda_{k,ij}^2 = \frac{\mathbf{L}_{ij}^2}{\sin^2\alpha_k} + \frac{\mathbf{L}_{k,ij}^2}{\cos^2\alpha_k}, \tag{9.}$$

where $\Omega = (\theta_{ij}, \phi_{ij}, \theta_{k,ij}, \phi_{k,ij})$ and the Ls in Equation 9 are the usual angular-momentum operators with respect to these angles.

We assume that the potential V depends only on the magnitude of the interparticle separation:

$$V(\mathbf{r}_1, \mathbf{r}_2, r_3) = V(r_{12}) + V(r_{23}) + V(r_{31}). \tag{10.}$$

We now employ the usual Faddeev decomposition of ψ for three identical bosons and neglect subsystem angular momentum:

$$\Psi(R, \alpha, \Omega) = \psi(R, \alpha_1) + \psi(R, \alpha_2) + \psi(R, \alpha_3). \quad 11.$$

The solution of the corresponding Faddeev equation can then be expanded in a set of eigenfunctions of the hyperangular operator; specifically,

$$\psi(R, \alpha) = \frac{1}{R^{5/2} \sin(2\alpha)} \sum_n f_n(R) \phi_n(R, \alpha). \quad 12.$$

This expansion leads to separate differential equations for the hyperangular functions ϕ_n and the hyperradial functions f_n. Particularly for the hyperradial functions, we obtain

$$\begin{aligned} E f_n(R) = &\left[\frac{\hbar^2}{2m} \left(-\frac{\partial^2}{\partial R^2} + \frac{15}{4R^2} \right) + V_n(R) \right] f_n(R) \\ &+ \sum_m \left[2P_{nm}(R) \frac{\partial}{\partial R} + Q_{nm}(R) \right] f_m(R), \end{aligned} \quad 13.$$

where the hyperradial potential $V_n(R)$ is defined by

$$V_n(R) = (\lambda_n(R) - 4) \frac{\hbar^2}{2mR^2}, \quad 14.$$

and $P_{nm}(R)$ and $Q_{nm}(R)$ are potentials that induce coupling between different hyperradial channels (1).

For hyperradii R, which are much larger than the range ℓ over which V is nonzero, the solution of the equation for the hyperangular function ϕ_n for large α is

$$\phi_n^{(\text{high})}(\alpha) \approx \sin\left[\sqrt{\lambda_n} \left(\frac{\pi}{2} - \alpha \right) \right]. \quad 15.$$

However, for $R \gg \ell$ and small α, the solution for the hyperangular part can be written as

$$\phi_n^{(\text{low})}(\alpha) = A \psi_0(\sqrt{2} R\alpha) - \frac{8\alpha}{\sqrt{3}} \sin\left(\sqrt{\lambda_n} \frac{\pi}{6} \right), \quad 16.$$

where A is a constant and ψ_0 is the zero-energy solution to a two-body Schrödinger equation with the two-body potential V,

$$\psi_k(r) = \frac{\sin[kr + \delta(k)]}{k} = \frac{\sin\delta(k)}{k} [\cos(kr) + \cot\delta \sin(kr)]. \quad 17.$$

As $k \to 0$, this expression yields $\psi_0(r) = r - a$, and we can use this asymptotic two-body wave function in Equation 16. This gives

$$\phi_n^{(\text{low})}(\alpha) = A(\sqrt{2} R\alpha - a) - \frac{8\alpha}{\sqrt{3}} \sin\left(\sqrt{\lambda_n} \frac{\pi}{6} \right). \quad 18.$$

Because $V = 0$ in this region, this result must be consistent with Equation 15. This is achieved by (*a*) choosing

$$A = -\frac{1}{a} \sin\left[\sqrt{\lambda_n} \frac{\pi}{2} \right], \quad 19.$$

which ensures that $\phi_n(\alpha)$ is continuous across the boundary between low and high solutions at $\alpha \approx \ell/R$, and (*b*) the condition

$$\cos\left(\sqrt{\lambda_n} \frac{\pi}{2} \right) - \frac{8}{\sqrt{3\lambda_n}} \sin\left(\sqrt{\lambda_n} \frac{\pi}{6} \right) = \sqrt{\frac{2}{\lambda_n}} \sin\left(\sqrt{\lambda_n} \frac{\pi}{2} \right) \frac{R}{a} \quad 20.$$

on λ_n, which ensures that $\phi_n(\alpha)$ has a continuous first derivative as $\alpha \to \ell/R$. We note that if these equations are satisfied, then λ_n, and hence ϕ_n, is independent of R for $R \ll |a|$. Indeed, as long as Equations 19 and 20 are satisfied, Equation 15 is the result for ϕ for all α, such that $\alpha > \ell/R$. Solving Equation 20 in the limit $R \ll |a|$ we find the lowest eigenvalue

$$\lambda_0 = -s_0^2 \left(1 + 1.897 \frac{R}{a}\right), \qquad 21.$$

where $s_0 = 1.00624\ldots$. This is the only negative eigenvalue, and therefore only this channel potential is attractive. If we now focus on the unitary limit, where $|a| \to \infty$, we have $\lambda_0 = -s_0^2$. Because it can also be shown that the coupling potentials P_{nm} and Q_{nm} vanish in this regime, the hyperradial equation (Equation 13) in the lowest channel becomes

$$\frac{\hbar^2}{2m}\left(-\frac{\partial^2}{\partial R^2} - \frac{s_0^2 + \frac{1}{4}}{R^2}\right) f_0(R) = E f_0(R). \qquad 22.$$

This equation holds for $R \gg \ell$. If we desire a solution for negative E, the requirement of normalizability for f_0 mandates that

$$f_0^{(0)}(R) = \sqrt{R} K_{is_0}(\sqrt{2}\kappa R), \qquad 23.$$

where the superscript (0) indicates that we are working in the unitary limit, and the subscript 0 refers to the solution for the hyperchannel corresponding to λ_0, which is the only one that supports bound states. The binding energy of these bound states is related to the κ of Equation 23 by

$$B_t \equiv \frac{\hbar^2 \kappa^2}{m}. \qquad 24.$$

Because the attractive $1/R^2$ potential produces a spectrum that is unbounded from below, some other short-distance physics is needed to stabilize the system. If the two-body potential is known, this short-distance physics is provided by the two-body potential V, which becomes operative for $R \sim \ell$. An alternative approach is to add an additional term to Equation 22 that summarizes the impact of the two-body V. We take this potential to be a surface δ function at a radius $1/\Lambda$ (29),

$$V_{SR}(R) = H_0(\Lambda)\Lambda^2 \delta\left(R - \frac{1}{\Lambda}\right), \qquad 25.$$

where H_0 is adjusted as a function of Λ such that the binding energy of a particular state, say $B_t^{(n_*)}$ (with a corresponding κ_*, given by Equation 24), is reproduced. Note that because V_{SR} is operative only at small hyperradii $R \sim 1/\Lambda$, it corresponds to a three-body force. (See Reference 30 for a realization of this in a momentum-space formalism.) In physical terms, we anticipate $\ell \sim 1/\Lambda$ because we know that once we consider hyperradii of order $1/\Lambda$, the potential V begins to affect the solutions.

Given that our focus is on predictions of the theory that are independent of details of V, we can consider the extreme case and take the limit $\ell \to 0$. In this limit, the form of K_{is_0} as $R \to 0$ guarantees that, once H_0 is fixed to give a bound state at $B_t^{(n_*)}$, the other binding energies in this hyperradial eigenchannel form a geometric spectrum. Specifically, $B_t^{(n)} = \hbar^2 \kappa_n^2/m$, where

$$\kappa_n = \left(e^{-\pi/s_0}\right)^{n-n_*} \kappa_*. \qquad 26.$$

Here n_* is the index of the bound state corresponding to κ_*. Equation 26 holds for all κ_n, such that $\kappa_n \ll \Lambda$. (Note that the subscript on κ now denotes the index of the bound state in adiabatic channel zero.) The continuous scale invariance of the $1/R^2$ potential has been broken down to a discrete scale invariance by the imposition of particular short-distance physics on the problem through the short-distance potential of Equation 25 (29).

The discrete scale invariance of the three-body wave function, which is exact in the limit of infinite scattering length and zero range, also has implications for finite range. A perturbative calculation of the effect of a finite effective range on the bound-state spectrum showed that the spectrum remains unchanged (31) and that corrections to binding energies are of order $(r_0/a)^2$, where r_0 is the effective range of the interaction.

2.3. Efimov Spectrum

The hyperspherical methods discussed above can also be used to obtain the binding energy spectrum at finite scattering length. The short-distance boundary condition that was used to fix the binding energy in the unitary limit also determines the bound-state spectrum at finite scattering length. The binding momentum κ_* introduced above can therefore be considered a convenient parameter that determines the value of all universal few-body observables of the corresponding universality class.

The exact discrete scaling symmetry observed in the limit of infinite scattering length also exists if κ_* is kept fixed and if a and other variables such as the energy are rescaled:

$$\kappa_* \to \kappa_*, \quad a \to \mathcal{S}_0^m a, \quad E \to \mathcal{S}_0^{-2m} E. \tag{27.}$$

Observables such as binding energy and cross sections scale with integer powers of $\mathcal{S}_0 = \exp(\pi/s_0)$ under this symmetry. For example, the binding energy of an Efimov state (trimer), which is a function of a and κ_*, scales as

$$B_t^{(n)}(\mathcal{S}_0^m a, \kappa_*) = \mathcal{S}_0^{-2m} B_t^{(n-m)}(a, \kappa_*). \tag{28.}$$

This implies for positive scattering length that

$$B_t^{(n)}(a, \kappa_*) = F_n[2s_0 \ln(a\kappa_*)] \frac{\hbar^2 \kappa_*^2}{m}. \tag{29.}$$

The function F_n parameterizes the scattering length dependency of all Efimov trimers exactly in the limit of vanishing range. The function F_n satisfies

$$F_n(x + 2m\pi) = (e^{-2\pi/s_0})^m F_{n-m}(x). \tag{30.}$$

The scattering length dependency of the bound-state spectrum is shown in **Figure 1**. We plot the quantity $K \equiv \mathrm{sgn}(E)(m|E|)^{1/2}/\hbar$ against the inverse scattering length (note that the axes have been rescaled such that the scaling factor is approximately 2.2 instead of 22.7). For bound states, K corresponds to the binding momentum. Only a few of the infinitely many Efimov branches are shown. A given physical system has a fixed scattering length value and is denoted by the vertical dashed line. Changing the parameter κ_* by a factor $\mathcal{S}_0$ corresponds to multiplying each branch of trimers with this factor without changing their shapes. One important result is that three-body bound states exist for positive and negative scattering lengths. This is remarkable for the latter case because the two-body subsystem is unbound for $a < 0$. At a negative scattering length that we denote with a'_*, a bound state with a given κ_* has zero binding energy. As the scattering length is increased, the binding energy increases until it crosses the atom-dimer threshold at the positive scattering length a_*. The quantities a_* and a'_* can also be used to quantify a universality class of Efimov states.

2.4. Universal Properties

Other calculable observables also display the discrete scaling symmetry discussed above for the bound-state spectrum. The atom-dimer cross section fulfills, for example, the constraint

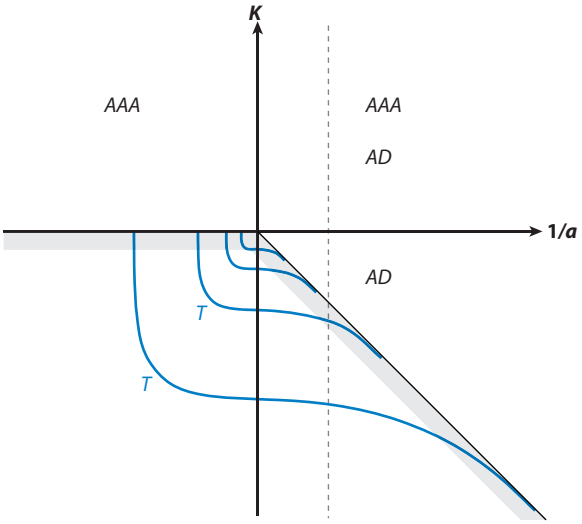

Figure 1

The Efimov plot for the three-body problem. We show $K \equiv \mathrm{sgn}(E)(m|E|)^{1/2}/\hbar$ versus the inverse scattering length. The allowed regions for three-atom scattering states and atom-dimer scattering states are labeled *AAA* and *AD*, respectively. The blue lines labeled *T* are two of the infinitely many branches of Efimov states. The gray shading indicates the threshold for scattering states. States along the vertical dashed line have a fixed scattering length. Adapted from Reference 1 with permission.

$$\sigma_{AD}(\mathcal{S}_0^{-2m}E;\mathcal{S}_0^m a,\kappa_*) = \mathcal{S}_0^{2m}\sigma_{AD}(E;a,\kappa_*) \qquad 31.$$

under rescaling. At $E = 0$, the cross section is related to the atom-dimer scattering length $\sigma_{AD} = 4\pi|a_{AD}|^2$. This relationship implies that the atom-dimer scattering length can be written as

$$a_{AD} = f[2s_0\ln(a\kappa_*)]a, \qquad 32.$$

where $f(x)$ is a periodic function with period 2π.

An observable that has been crucial for the experimental detection of Efimov physics in ultracold atoms is the three-body recombination rate. In ultracold gases, atoms can undergo inelastic three-body collisions in which a two-body bound state is formed. The dimer and remaining atom gain kinetic energy in this process and can leave the atomic trap. Such processes lead to a measurable loss of particles in the atomic trap. For negative scattering length, atoms can only recombine into deep dimers that have binding energy of order $\hbar^2/(mR^2)$. For positive scattering length, atoms can recombine into (*a*) shallow dimers with binding energy $\hbar^2/(ma^2)$ and (*b*) deep dimers. The recombination rate that is a measure for the loss rate of atoms scales as $\hbar a^4/m$ multiplied by a log-periodic coefficient that is a function of a and κ_*. The recombination rate constant α can therefore be written as

$$\alpha(a) = g[2s_0\ln(a\kappa_*)]\frac{\hbar a^4}{m}. \qquad 33.$$

The analytic form of the function $g(x)$ is known and can be found in References 1 and 6. Here we focus on the qualitative features of positive scattering length (**Figure 2**). At positive scattering length, interference effects lead to log-periodically spaced minima in the recombination rate. At negative scattering length, free atoms can only recombine into deep dimers. This process is enhanced dramatically whenever an Efimov trimer is at threshold.

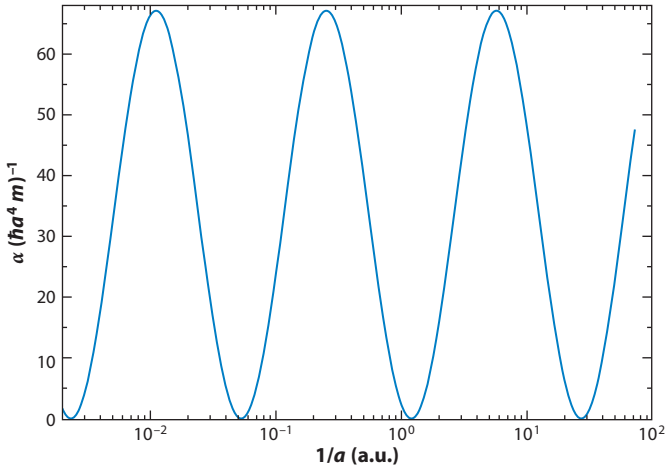

Figure 2

The recombination rate constant α for positive scattering length a in units of $\hbar a^4/m$ as a function of $1/a$ (in arbitrary units).

A different perspective on Efimov physics can be gained by keeping the two-body scattering length fixed and varying the three-body parameter. As a result, all three-body observables are correlated and lead to correlation lines when plotted against each other. One of these lines is the Phillips line (32): the correlation that results when the trimer binding energy is plotted against the atom-dimer scattering length. Such correlations have frequently been observed in nuclear physics, in which different phase-shift equivalent potentials are employed in few-body calculations.

Because one three-body parameter is required for a description of the three-body system with zero-range interactions, one must determine how many parameters are needed for calculations in the n-body system. A first step toward answering this question was taken in Reference 33. The authors of this work showed that the two-body scattering length and one three-body parameter are sufficient to make predictions for four-body observables. Results in a more detailed analysis (34) led to the conclusion that every trimer state is tied to two universal tetramer states with binding energies related to the binding energy of the next-shallower trimer. In the unitary limit $1/a = 0$, the relation between the binding energies is

$$B_4^{(0)} \approx 5\,B_t \quad \text{and} \quad B_4^{(1)} \approx 1.01\,B_t, \qquad 34.$$

where $B_4^{(0)}$ denotes the binding energy of the deeper of the two tetramer states and $B_4^{(1)}$ denotes the binding energy of the shallower of the two.

A recent calculation by von Stecher et al. (35) supports these findings and extends them to higher numerical accuracy. For the relation between universal three- and four-body bound states in the unitary limit, the authors found that

$$B_4^{(0)} \approx 4.57\,B_t \quad \text{and} \quad B_4^{(1)} \approx 1.01\,B_t, \qquad 35.$$

which is consistent with the results given in Equation 34 within the numerical accuracy.

The results obtained by Hammer & Platter (34) were presented in the form of an extended Efimov plot (**Figure 3**). Four-body states must have a binding energy larger than that of the deepest trimer state. An extended version of this four-body Efimov plot was also presented by von Stecher et al. (35). The authors of this study calculated more states with higher numerical accuracy and extended the calculation of the four-body states to the thresholds at which they

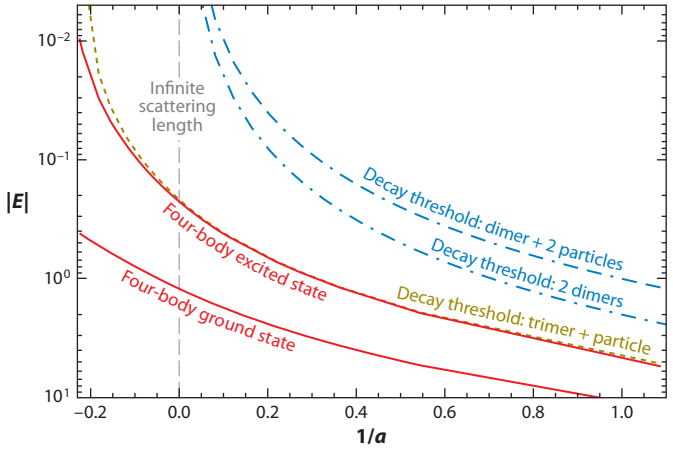

Figure 3

The extended Efimov plot for the four-body problem. Shown is the absolute value of energy E versus the inverse scattering length. Both quantities are given in arbitrary units. The lower (upper) solid red line denotes the four-body ground (excited) state. The dashed dark yellow line represents the threshold for decay into a ground-state trimer and a particle. The lower (upper) blue dashed-dotted line represents the threshold for decay into two dimers (a dimer and two particles). The vertical dashed line indicates the infinite scattering length.

become unstable. From these results, they extracted the negative values of the scattering lengths at which the binding energies of the tetramer states become zero and found that

$$a^*_{4,0} \approx 0.43 a'_* \quad \text{and} \quad a^*_{4,1} \approx 0.92 a'_*. \qquad 36.$$

These numbers uniquely specify the relative position of three- and four-body recombination resonances. This information was essential for Ferlaino et al.'s (36) subsequent observation of these states in ultracold atoms.

Calculations for larger numbers of particles by means of a model that incorporates the universal behavior of the three-body system were carried out by von Stecher (37). His findings indicate that there is at least one n-body state tied to each Efimov trimer, and he also found numerical evidence for a second excited five-body state.

2.5. Observation in Ultracold Atoms

The first experimental evidence for Efimov physics in ultracold atoms was presented by Kraemer et al. (5) in 2006. This group used ^{133}Cs atoms in the lowest hyperfine spin state. They observed resonant enhancement of the loss of atoms from three-body recombination that can be attributed to an Efimov trimer crossing the three-atom threshold. Kraemer et al. also observed a minimum in the three-body recombination rate that can be interpreted as an interference effect associated with Efimov physics. In a subsequent experiment with a mixture of ^{133}Cs atoms and dimers, Knoop et al. (38) observed a resonant enhancement in the loss of atoms and dimers. This loss feature can be explained by an Efimov trimer crossing the atom-dimer threshold (39). The most exciting recent developments in the field of Efimov physics involve universal tetramer states. Ferlaino et al. (36) observed two tetramers in an ultracold gas of ^{133}Cs atoms that confirm the results by Platter et al. (33), Hammer & Platter (34), and von Stecher et al. (35).

Recent experiments with other bosonic atoms have provided even stronger evidence of Efimov physics in the three- and four-body sectors. Zaccanti et al. (40) measured the three-body recombination rate and the atom-dimer loss rate in an ultracold gas of ^{39}K atoms. They observed two atom-dimer loss resonances and two minima in the three-body recombination rate at large positive values of the scattering length. The positions of the loss features are consistent with the universal predictions, with a discrete scaling factor of 22.7. Zaccanti et al. also observed loss features at large negative scattering lengths. Barontini et al. (41) obtained the first evidence of the Efimov effect in a heteronuclear mixture of ^{41}K and ^{87}Rb atoms. They observed three-atom loss resonances at large negative scattering lengths in both the K-Rb-Rb and K-K-Rb channels, for which the discrete scaling factors are 131 and 3.51×10^5, respectively. Gross et al. (42) measured the three-body recombination rate in an ultracold system of ^{7}Li atoms. They observed a three-atom loss resonance at a large negative scattering length and a three-body recombination minimum at a large positive scattering length. The positions of the loss features, which are in the same universal region on different sides of a Feshbach resonance, are consistent with the universal predictions, with a discrete scaling factor of 22.7. Pollack et al. (43) measured the three-body recombination in a system of ^{7}Li atoms in a hyperfine state different from the system considered by Gross et al. Pollack et al. (43) observed a total of 11 three- and four-body loss features. The features obey the universal relations on each side of the Feshbach resonance separately; however, a systematic deviation of 50% is found when features on different sides of the Feshbach resonance are compared.

Efimov physics has also been observed in three-component systems of the ^{6}Li atom. For the three lowest hyperfine states of ^{6}Li atoms, the three-pair scattering lengths approach a common large negative value at large magnetic fields, and all three have nearby Feshbach resonances at lower fields that can be used to vary the scattering lengths (44). The first experimental studies of many-body systems of ^{6}Li atoms in the three lowest hyperfine states have recently been carried out by Ottenstein et al. (45) and by Huckans et al. (46). These groups' measurements of the three-body recombination rate revealed a narrow loss feature and a broad loss feature in a region of low magnetic field. Theoretical calculations of the three-body recombination rate supported the interpretation that the narrow loss feature arises from an Efimov trimer crossing the three-atom threshold (47–49). Very recently, another narrow loss feature was discovered in a much higher region of the magnetic field by Williams et al. (50) and by Jochim and coworkers (51). Williams et al. used measurements of the three-body recombination rate in this region to determine the complex three-body parameter that governs Efimov physics in this system. This parameter, together with the three scattering lengths as functions of the magnetic field, determines the universal predictions for ^{6}Li atoms in this region of the magnetic field.

3. APPLICATIONS IN NUCLEAR PHYSICS

The properties of hadrons and nuclei are determined by quantum chromodynamics (QCD), a nonabelian gauge theory formulated in terms of quark and gluon degrees of freedom. At low energies, however, the appropriate degrees of freedom are the hadrons. Efimov physics and the unitary limit can serve as a useful starting point for EFTs that describe hadrons and nuclei at very low energies. For convenience, we work in natural units, where $\hbar = c = 1$.

In nuclear physics, there are a number of EFTs, all of which are useful for a certain range of systems (52–54). At very low energies, where Efimov physics plays a role, all interactions can be considered short range, and even the pions can be integrated out. This so-called pionless EFT is formulated in an expansion of the low-momentum scale M_{low} over the high-momentum scale M_{high}. It can be understood as an expansion around the limit of infinite scattering length

or, equivalently, around near-threshold bound states. Its breakdown scale is set by a one-pion exchange, $M_{high} \sim M_\pi$, whereas $M_{low} \sim 1/a \sim k$. For momenta k of the order of the pion mass M_π, pion exchange becomes a long-range interaction and has to be treated explicitly. Doing so leads to the chiral EFT, whose breakdown scale M_{high} is set by the chiral symmetry–breaking scale Λ_χ. The pionless theory relies only on the large scattering length and is independent of the short-distance mechanism generating it. This theory is therefore ideally suited to unraveling universal phenomena driven by the large scattering length, such as limit-cycle physics (55, 56) and the Efimov effect (3). In this section, we focus on the aspects of nuclear EFTs related to Efimov physics. More complete overviews of the application of EFTs to nuclear phenomena in general are available (52–54, 57).

3.1. Few-Nucleon Systems

In the two-nucleon system, the pionless theory reproduces the well-known effective range expansion in the large scattering length limit. The renormalized S-wave scattering amplitude to next-to-leading order (NLO) in a given channel takes the form

$$T_2(k) = \frac{4\pi}{m}\frac{1}{-1/a - ik}\left[1 - \frac{r_0 k^2/2}{-1/a - ik} + \ldots\right], \qquad 37.$$

where k is the relative momentum of the nucleons and the dots indicate corrections of order $(M_{low}/M_{high})^2$ for typical momenta $k \sim M_{low}$. In the language of the renormalization group, Equation 37 corresponds to an expansion around the nontrivial fixed point for $1/a = 0$ (58, 59). The pionless EFT becomes very useful in the two-nucleon sector when external currents are considered, and it has been applied to a variety of electroweak processes. These calculations are reviewed in detail in References 52 and 53.

Here we focus on the three-nucleon system. It is convenient (but not mandatory) to write the theory using so-called dimeron auxiliary fields (60). We need two dimeron fields, one for each S-wave channel: (*a*) a field t_i with spin (isospin) 1 (0) representing two nucleons interacting in the $^3S_1$ channel (the deuteron) and (*b*) a field s_a with spin (isospin) 0 (1) representing two nucleons interacting in the $^1S_0$ channel (23). Specifically,

$$\begin{aligned}\mathcal{L} = {} & N^\dagger\left(i\partial_t + \frac{\vec{\nabla}^2}{2m}\right)N - t_i^\dagger\left(i\partial_t + \frac{\vec{\nabla}^2}{4m} - \Delta_t\right)t_i \\ & - s_a^\dagger\left(i\partial_t + \frac{\vec{\nabla}^2}{4m} - \Delta_s\right)s_a - \frac{g_t}{2}\left(t_i^\dagger N^T \tau_2\sigma_i\sigma_2 N + \text{h.c.}\right) \\ & - \frac{g_s}{2}\left(s_a^\dagger N^T \sigma_2\tau_a\tau_2 N + \text{h.c.}\right) - G_3 N^\dagger\left[g_t^2(t_i\sigma_i)^\dagger(t_j\sigma_j)\right. \\ & \left. + \frac{g_t g_s}{3}\left((t_i\sigma_i)^\dagger(s_a\tau_a) + \text{h.c.}\right) + g_s^2(s_a\tau_a)^\dagger(s_b\tau_b)\right]N + \ldots, \end{aligned} \qquad 38.$$

where i and j are spin; a and b are isospin indices; and g_t, g_s, Δ_t, Δ_s, and G_3 are the bare coupling constants. The Pauli matrices σ_i (τ_a) operate in spin (isospin) space. This Lagrangian goes beyond leading order (LO) and already includes the effective range terms. The coupling constants g_t, Δ_t, g_s, and Δ_s, are matched to the scattering lengths a_α and effective ranges $r_{0\alpha}$ in the two channels ($\alpha = s, t$). Alternatively, one can match to the position of the bound-state/virtual-state pole γ_α in the T-matrix instead of the scattering length, which often improves convergence (61).

The term proportional to G_3 constitutes a Wigner $SU(4)$ symmetric three-body interaction. It only contributes in the spin-doublet S-wave channel. When the auxiliary dimeron fields t_i and s_a are integrated out, an equivalent form containing only nucleon fields is obtained. At LO, when the

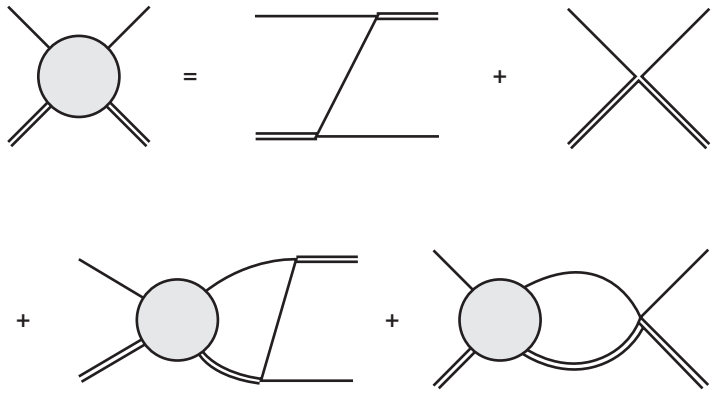

Figure 4

The integral equation for the particle-dimeron scattering amplitude. The single (double) line indicates the particle (dimeron) propagator. Adapted from Reference 1 with permission.

effective range corrections are neglected, the spatial and time derivatives acting on the dimeron fields are omitted and the field is static. The coupling constants g_α and Δ_α, $\alpha = s, t$ are then not independent, and only the combination g_α^2/Δ_α enters in observables. This combination can then be matched to the scattering length or pole position.

The simplest three-body process to consider is neutron-deuteron scattering below the breakup threshold. To focus on the main aspects of renormalization, we suppress all spin-isospin indices and complications from coupled channels in the three-nucleon problem. The resulting system is equivalent to a system of three spinless bosons with large scattering length. If the scattering length is positive, the particles form a two-body bound state analog to the deuteron, which we generically term a dimeron. The LO integral equation for particle-dimeron scattering is shown schematically in **Figure 4**. Projected on total orbital angular momentum $L = 0$, it takes the form

$$T_3(k, p; E) = \frac{16}{3a} M(k, p; E) + \frac{4}{\pi} \int_0^\Lambda dq\, q^2\, T_3(k, q; E) \times \frac{M(q, p; E)}{-1/a + \sqrt{3q^2/4 - mE - i\epsilon}}, \tag{39.}$$

where the inhomogeneous term reads

$$M(k, p; E) = \frac{1}{2kp} \ln\left(\frac{k^2 + kp + p^2 - mE}{k^2 - kp + p^2 - mE}\right) + \frac{H(\Lambda)}{\Lambda^2}. \tag{40.}$$

Here $H(\Lambda)$ is a running coupling constant that determines the strength of the three-body force $G_3(\Lambda) = 2mH(\Lambda)/\Lambda^2$, and Λ is a UV cutoff introduced to regularize the integral equation. Note that the three-body force is enhanced and enters at LO in this theory. The magnitude of the incoming (outgoing) relative momenta is k (p), and $E = 3k^2/(4m) - 1/(ma^2)$. The on-shell point corresponds to $k = p$, and the phase shift can be obtained via $k \cot \delta = 1/T_3(k, k; E) + ik$. For $H \equiv 0$ and $\Lambda \to \infty$, Equation 39 reduces to the STM (Skorniakov–Ter-Martirosian) equation (8). It is well known that the STM equation has no unique solution (9). The regularized STM equation has a unique solution for any given (finite) value of the UV cutoff Λ, but the solution strongly depends on the value of Λ. In the EFT framework, cutoff independence of the amplitude is achieved by an appropriate "running" of $H(\Lambda)$ (30, 62),

$$H(\Lambda) = \frac{\cos[s_0 \ln(\Lambda/\Lambda_*) + \arctan s_0]}{\cos[s_0 \ln(\Lambda/\Lambda_*) - \arctan s_0]}, \tag{41.}$$

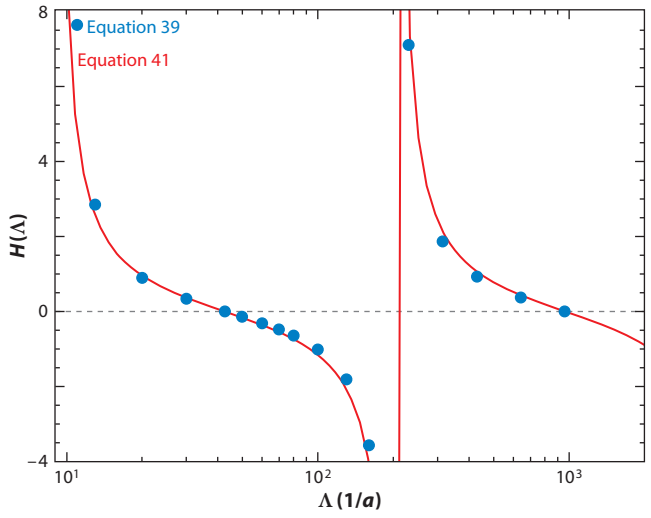

Figure 5

The three-body coupling H as a function of the cutoff Λ for a fixed value of the three-body parameter Λ_*. The solid red line shows the analytical expression from Equation 41, whereas the blue dots show results from the numerical solution of Equation 39.

where Λ_* is a dimensionful three-body parameter generated by dimensional transmutation. The dependence of the three-body coupling H on the cutoff Λ is shown in **Figure 5** for a fixed value of the three-body parameter Λ_*. A good agreement between the methods of Equations 39 and 41 is observed, indicating that the renormalization is well under control. Adjusting Λ_* to a single three-body observable allows us to determine all other low-energy properties of the three-body system.[1] Because $H(\Lambda)$ in Equation 41 vanishes for certain values of the cutoff Λ, it is possible to eliminate the explicit three-body force from the equations by working with a fixed cutoff that encodes the dependency on Λ_*. Doing so justifies tuning the cutoff Λ in the STM equation to reproduce a three-body datum and using the same cutoff to calculate other observables, as suggested by Kharchenko (63). Equivalently, a subtraction can be performed in the integral equation (64, 65). In all cases, one three-body input parameter is needed for the calculation of observables.

The discrete scaling symmetry of the Efimov spectrum is manifest in the running of the coupling $H(\Lambda)$. The spectrum of three-body bound states of this EFT is exactly the Efimov spectrum. The integral equations for the three-nucleon problem derived from the Lagrangian (Equation 38) are a generalization of Equation 39. (For their explicit form and derivation, see, e.g., Reference 66.)

For S-wave nucleon-deuteron scattering in the spin-quartet channel, only the spin-1 dimeron field contributes, and the integral equation becomes (8, 21, 22)

$$T_3^{(3/2)}(p,k;E) = -\frac{4\gamma_t}{3}K(p,k) - \frac{1}{\pi}\int_0^\infty dq\, q^2 D_t(q;E)K(p,q)T_3^{(3/2)}(q,k;E), \qquad 42.$$

where

$$K(p,k) = \frac{1}{pk}\ln\left(\frac{p^2+pk+k^2-mE}{p^2-pk+k^2-mE}\right), \qquad 43.$$

$D_t(q;E)$ is the full spin-1 dimeron propagator, and $\gamma_t \approx 45$ MeV is the deuteron pole momentum.

[1]Note that the choice of the three-body parameter Λ_* is not unique. For alternative definitions, see Reference 1.

This integral equation has a unique solution for $\Lambda \to \infty$, and there is no three-body force in the first few orders. An S-wave three-body force is forbidden by the Pauli principle in this channel because all nucleon spins must be aligned to obtain $J = 3/2$. The spin-quartet scattering phases $k \cot \delta^{(3/2)} = 1/T_3^{(3/2)}(k, k; E) + ik$ can therefore be predicted to high precision from two-body data alone.

In the spin-doublet channel, both dimeron fields as well as the three-body force in the Lagrangian (Equation 38) contribute (23). This contribution leads to a pair of coupled integral equations for the T-matrix. The renormalization of this equation is easily understood in the unitary limit, which corresponds to a Wigner $SU(4)$ symmetry of the theory (Equation 24). In the unitary limit, these two integral equations decouple. One of the two equations has the same structure as the equation for the bosonic problem (Equation 39), whereas the other one is similar to the equation in the quartet channel (Equation 42). Thus, one needs a new parameter that is not determined in the two-nucleon system in order to fix the (leading) low-energy behavior of the three-nucleon system in this channel. This parameter corresponds to the $SU(4)$ symmetric three-body force proportional to G_3 in the Lagrangian (Equation 38) (23). The three-body parameter gives a natural explanation of universal correlations between different three-body observables such as the Phillips line, a correlation between the triton binding energy and the spin-doublet neutron-deuteron scattering length (32). These correlations are driven purely by the large scattering length, independent of the mechanism responsible for it. If the spin-doublet neutron-deuteron scattering length is given, the triton binding energy is predicted. In this scenario, the triton emerges as an Efimov state. This scenario can be tested by using the effective theory to predict other three-body observables.

Higher-order corrections to the amplitude, including those due to two-nucleon effective range terms, can be included perturbatively. This was first done at NLO for the scattering length and triton binding energy (20) and for the energy dependency of the phase shifts (64). The authors of References 66 and 67 demonstrated that it is convenient to iterate certain higher-order range terms to extend the calculation to next-to-next-to-leading order (NNLO). Here a subleading three-body force was also included, as required by dimensional analysis. More recently, Platter & Phillips (68) showed, using the subtractive renormalization, that the leading three-body force is sufficient to achieve cutoff independence up to NNLO in the expansion in M_{low}/M_{high}. The results for the spin-doublet neutron-deuteron scattering phase shift at LO (23), NLO (64), and NNLO (69) are shown in **Figure 6**. There is excellent agreement with the available phase-shift analysis and a calculation that uses a phenomenological nucleon-nucleon interaction. From dimensional analysis, one would expect the subleading three-body force at NNLO. Whether there is a suppression of the subleading three-body force or simply a correlation between the leading and subleading contributions is not understood.

Three-nucleon channels with higher orbital angular momentum are similar to the spin quartet for S-waves, and three-body forces do not appear until very high orders (70). A general counting scheme for three-body forces based on the asymptotic behavior of the solutions of the LO STM equation was proposed by Griesshammer (71). A complementary approach to the few-nucleon problem is given by the renormalization group, in which the power counting is determined from the scaling of operators under the renormalization group transformation (72). This method leads to consistent results for the power counting (73–75).

Three-body calculations with external currents are still in their infancy. However, a few exploratory calculations have been carried out. Universal properties of the triton charge form factor have been investigated (76), and neutron-deuteron radiative capture has been calculated (77–79). The electromagnetic properties of the triton were also recently investigated (80, 81). This work raises the possibility of carrying out accurate calculations of electroweak reactions at very low energies for astrophysical processes.

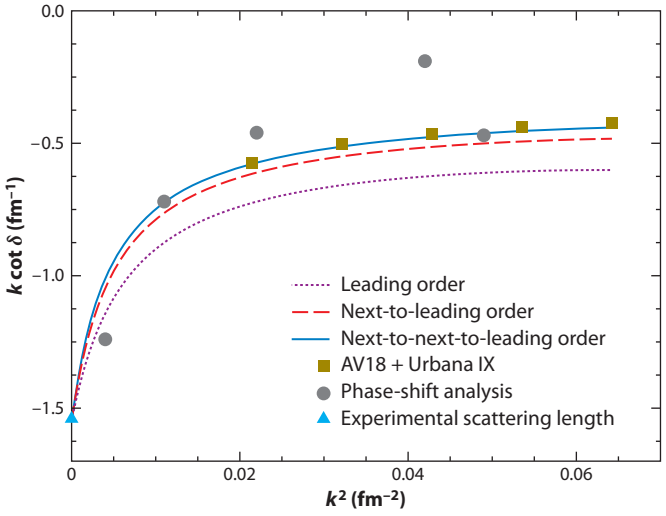

Figure 6

Phase shifts for neutron-deuteron scattering below the deuteron breakup at leading order (*purple dotted line*), next-to-leading order (*red dashed line*), and next-to-next-to-leading order (*solid blue line*). The dark yellow squares and gray circles represent the results of a phase-shift analysis and a calculation that used AV18 and the Urbana IX three-body force, respectively. The light blue triangle represents the experimental scattering length. Adapted from Reference 69 with permission.

The pionless approach has also been extended to the four-body sector (33, 82). To be able to apply the Yakubovsky equations, the authors used an equivalent effective quantum mechanics formulation. The study of the cutoff dependency of the four-body binding energies revealed that no four-body parameter is required for renormalization at LO. As a consequence, there are universal correlations in the four-body sector that are also driven by the large scattering length. The best-known example is the Tjon line: a correlation between the triton and α particle binding energies, B_t and B_α, respectively. Of course, higher-order corrections break the exact correlation and generate a band. In **Figure 7**, we show this band together with some calculations that make use of phenomenological potentials (83) and a chiral EFT potential with explicit pions (84, 85). All calculations with interactions that give a large scattering length must lie within the band. Different short-distance physics and/or cutoff dependency should only move the results along the band. This can be observed, for example, in the NLO results with the chiral potential indicated by the squares in **Figure 7** or in the few-body calculations with the low-momentum nucleon-nucleon potential $V_{\mathrm{low\ k}}$ (86). The $V_{\mathrm{low\ k}}$ potential is obtained from phenomenological nucleon-nucleon interactions by integrating out high-momentum modes above a cutoff Λ but leaving two-body observables (such as the large scattering lengths) unchanged. The results of few-body calculations with $V_{\mathrm{low\ k}}$ are not independent of Λ but lie close to the Tjon line (cf. figure 2 of Reference 86).

Another interesting development is the application of the resonating group model to solve the pionless EFT for three- and four-nucleon systems (87). This method allows for a straightforward inclusion of Coulomb effects. Kirscher et al. (87) extended previous calculations in the four-nucleon system to NLO and showed that the Tjon line correlation persists. Moreover, they calculated the correlation between the singlet S-wave ^{3}He-neutron scattering length and the triton binding energy. Preliminary results for the halo nucleus ^{6}He have been reported (88).

The pionless theory has also been applied within the no-core shell model framework. Here the expansion in a truncated harmonic oscillator basis is used as the UV regulator of the EFT. The

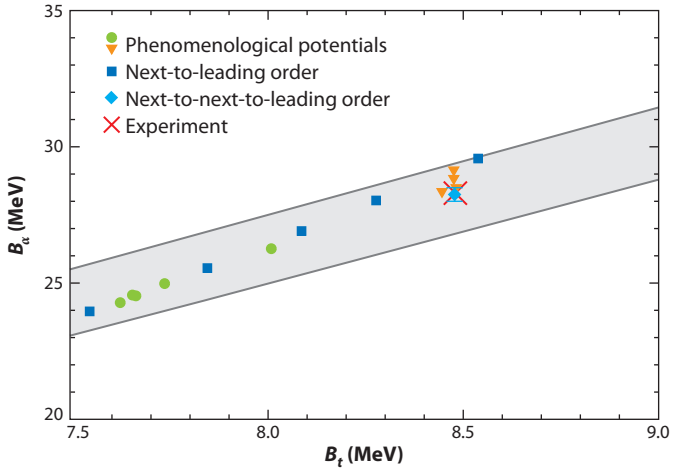

Figure 7

The Tjon line correlation as predicted by the pionless theory. The colored circles and triangles represent various calculations that use phenomenological potentials (83). The dark blue squares represent the results of a chiral effective field theory at next-to-leading order for different cutoffs, whereas the light blue diamond represents the next-to-next-to-leading order result (84, 85). The red cross indicates the experimental point. Adapted from Reference 82 with permission.

effective interaction is determined directly in the model space, where an exact diagonalization in a complete many-body basis is performed. The authors of Reference 89 calculated the 0^+ excited state of ^{4}He and the ^{6}Li ground state using the deuteron, triton, and α particle ground states as input. The first 0^+ excited state in ^{4}He was calculated within 10% of the experimental value, whereas the ^{6}Li ground state was approximately 70% of the experimental value, in agreement with the 30% error expected for the LO approximation. These results are promising and should be improved if range corrections are included. Finally, the spectrum of trapped three- and four-fermion systems was calculated with the same method (90). In this case, the harmonic potential is physical and not simply used as an UV regulator. For an update on this work, see Reference 91.

3.2. Quark Mass Dependence and Infrared Limit Cycle

In the following paragraphs, we discuss the possibility of an exact infrared limit cycle and the Efimov effect in a deformed version of QCD with quark masses slightly larger than their physical values. The quark mass dependency of the chiral nucleon-nucleon interaction was calculated to NLO in the chiral counting (92, 93). At this order, the quark mass dependency is synonymous with the pion mass dependency because of the Gell-Mann–Oakes–Renner relation: $M_\pi^2 = -(m_u + m_d)\langle 0|\bar{u}u|0\rangle / F_\pi^2$, where $\langle 0|\bar{u}u|0\rangle \approx (-290\,\mathrm{MeV})^3$ is the quark condensate. In this section, we therefore use the term pion mass dependency instead of quark mass dependency, which is more convenient for our purpose. The pion mass dependency of the nucleon-nucleon scattering lengths in the $^3S_1$–$^3D_1$ and $^1S_0$ channels, as well as the deuteron binding energy, has been calculated 92–94.

In principle, the pion mass dependence of the chiral nucleon-nucleon potential is determined uniquely. However, the extrapolation away from the physical pion mass generates errors. The dominating sources are the constants $\bar{C}_{S,T}$ and $\bar{D}_{S,T}$, which give the corrections to the LO contact terms $\propto M_\pi^2$ and cannot be determined independently from fits to data at the physical pion mass. A smaller effect is due to the error in the low-energy constant $\bar{d}_{16}$, which governs the pion mass

dependence of g_A. Both effects generate increasing uncertainties as one extrapolates away from the physical point.

In the calculation given in Reference 93, the size of the two constants $\bar{D}_S$ and $\bar{D}_T$ was constrained from naturalness arguments, assuming that $-3 \leq F_\pi^2 \Lambda_\chi^2 \bar{D}_{S,T} \leq 3$, where $\Lambda_\chi \simeq 1$ GeV is the chiral symmetry–breaking scale. These bounds are in agreement with resonance saturation estimates (95). The constant $\bar{d}_{16}$ was varied in the range $\bar{d}_{16} = -0.91 \ldots -1.76$ GeV^{-2} (96). This range was used to estimate the extrapolation errors of two-nucleon observables such as the deuteron binding energy and the spin-singlet and spin-triplet scattering lengths (93). In the chiral limit, the deuteron binding energy was found to be of natural size: $B_d \sim F_\pi^2/m \simeq 10$ MeV. Note, however, that if larger uncertainties in the low-energy constants $\bar{D}_S$ and $\bar{D}_T$ are assumed, one cannot make a definite statement about the binding of the deuteron in the chiral limit (92, 94). For pion masses above the physical value, however, all calculations show similar behavior.

In **Figure 8**, we show the inverse scattering lengths in the spin-triplet and spin-singlet channels from Reference 93, together with some recent lattice results from Reference 99. **Figure 8** also shows that a scenario in which both inverse scattering lengths vanish simultaneously at a critical pion mass of approximately 200 MeV is possible. For pion masses below the critical value, the spin-triplet scattering length is positive and the deuteron is bound. As the inverse spin-triplet scattering length decreases, the deuteron becomes more and more shallow and finally becomes unbound at the critical mass. Above the critical pion mass, the deuteron exists as a shallow virtual state. In the spin-singlet channel, the situation is reversed: The spin-singlet deuteron is a virtual state below the critical pion mass and becomes bound above. On the basis of this behavior, Braaten & Hammer (56) conjectured that one should be able to reach the critical point by varying the up and down quark masses m_u and m_d independently because the spin-triplet and spin-singlet channels have different isospin. In this case, the triton would display the Efimov effect, which corresponds to the occurrence of an infrared limit cycle in QCD. A complete investigation of

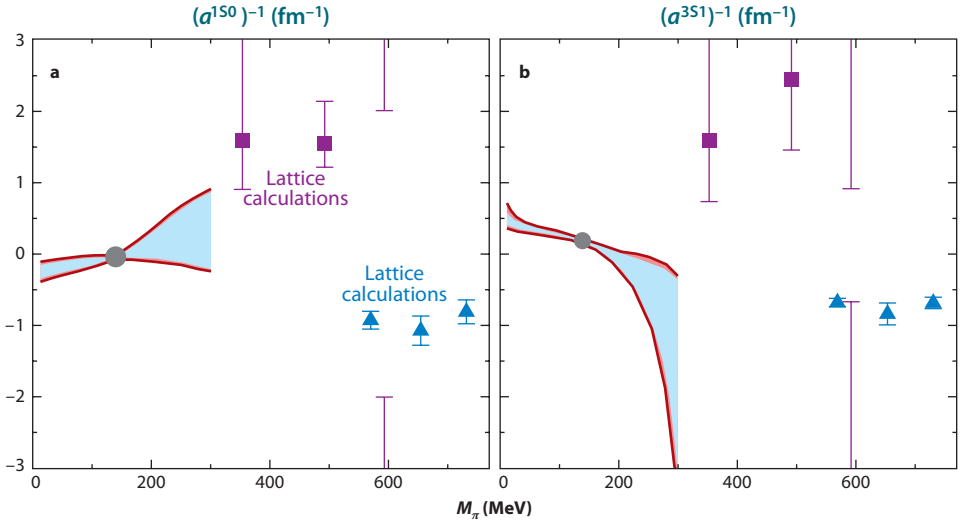

Figure 8

Inverse of the S-wave scattering lengths in the (*a*) spin-singlet and (*b*) spin-triplet nucleon-nucleon channels as a function of the pion mass M_π. The blue triangles represent the lattice calculations from References 97 and 98; the purple squares represent those from Reference 99. Adapted from Reference 54 with permission.

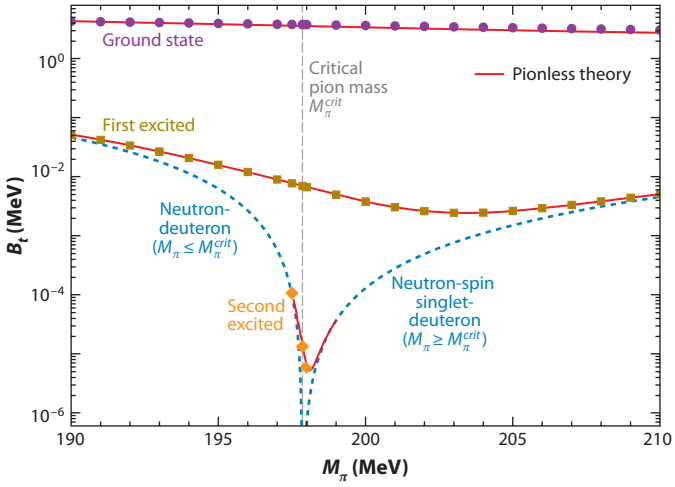

Figure 9

Binding energies B_t of the triton ground state and first two excited states as a function of M_π. The circles, squares, and diamonds represent the chiral effective field theory result, and the solid red lines represent calculations in the pionless theory. The vertical gray dotted line indicates the critical pion mass M_π^{crit}, and the dashed blue lines are the neutron-deuteron ($M_\pi \leq M_\pi^{crit}$) and neutron–spin singlet–deuteron ($M_\pi \geq M_\pi^{crit}$) bound-state thresholds. Adapted from Reference 101 with permission.

this issue requires the inclusion of isospin-breaking corrections and therefore higher orders in the chiral EFT. However, the universal properties of the limit cycle have been investigated by considering specific values of $\bar{D}_S$ and $\bar{D}_T$ that lie within the naturalness bound and that cause the spin-singlet and spin-triplet scattering lengths to become infinite at the same value of the pion mass.

The properties of the triton around the critical pion mass have been studied for one particular solution with a pion mass, M_π^{crit}, of197.8577 MeV (100). From the solution of the Faddeev equations, the binding energies of the triton and the first two excited states in the vicinity of the limit cycle were calculated for this scenario in chiral EFT. The binding energies are given in **Figure 9**. The neutron-deuteron ($M_\pi \leq M_\pi^{crit}$) and neutron–spin singlet–deuteron ($M_\pi \geq M_\pi^{crit}$) thresholds are also shown. Directly at the critical mass, these thresholds coincide with the three-body threshold, and the triton has infinitely many excited states. **Figure 9** also shows the LO calculations in the pionless theory that use the pion mass dependence of the nucleon-nucleon scattering lengths and one triton state from chiral EFT as input. The chiral EFT results for the other triton states in the critical region are reproduced very well. The binding energy of the triton ground state varies only weakly over the whole range of pion masses and is approximately one-half of the physical value at the critical point. The excited states are strongly influenced by the thresholds and vary much more strongly.

These studies have been extended to NNLO in the pionless EFT and neutron-deuteron scattering observables (101). The higher-order corrections in the vicinity of the critical pion mass are small. This is illustrated in **Figure 10**.

A final answer to the question of whether an infrared limit cycle can be realized in QCD can be obtained only by solving QCD directly. Determining whether this solution can be achieved by appropriately tuning the quark masses in a lattice QCD simulation (102) would be particularly interesting. The first full lattice QCD calculation of nucleon-nucleon scattering has been reported (99), but statistical noise presented a serious challenge. A promising recent high-statistics study of

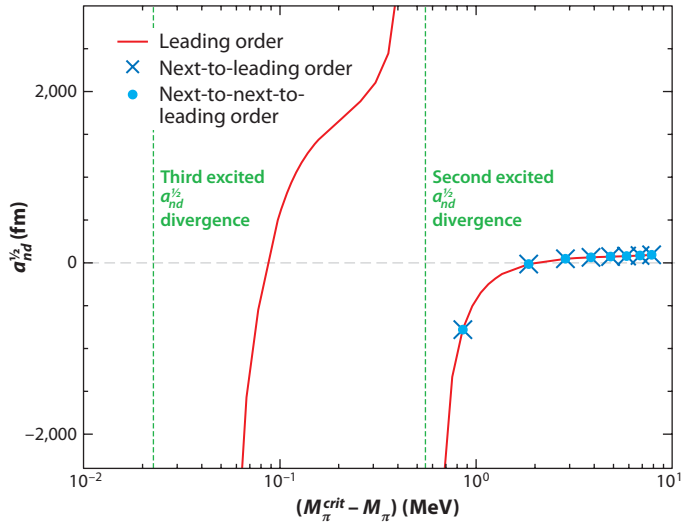

Figure 10

Doublet neutron-deuteron scattering length $a_{nd}^{1/2}$ in the critical region computed in the pionless effective field theory. The solid red line represents the leading-order result, and the light blue crosses and dark blue circles represent the next-to-leading order and next-to-next-to-leading order results, respectively. The vertical green dotted lines indicate the pion masses at which $a_{nd}^{1/2}$ diverges because the second and third excited states of the triton appear at the neutron-deuteron threshold. These singularities in $a_{nd}^{1/2}(M_\pi)$ are a clear signature that the limit cycle is approached in the critical region. Adapted from Reference 101 with permission.

three-baryon systems also presented initial results for a system with the quantum numbers of the triton, such that lattice QCD calculations of three-nucleon systems are now within sight (103). For a review of these activities, see Reference 104.

Such calculations require a detailed understanding of the modification of the Efimov spectrum in a cubic box. For identical bosons, there are significant finite volume shifts even for moderate box sizes (105). These shifts show universal scaling behavior that could be exploited to reduce the computational effort (106). The extension of these studies to the triton case is in progress.

3.3. Halo Nuclei

A special class of nuclear systems exhibiting universal behavior consists of halo nuclei (27, 107). A halo nucleus comprises a tightly bound core surrounded by one or more loosely bound valence nucleons. The valence nucleons are characterized by a very low separation energy compared with those in the core. As a consequence, the radius of the halo nucleus is large compared with the radius of the core. A trivial example is the deuteron, which can be considered a two-body halo nucleus. The root mean square radius of the deuteron is approximately three times larger than that of the constituent nucleons. Halo nuclei with two valence nucleons are particularly interesting examples of three-body systems. If none of the two-body subsystems is bound, the halo nuclei are termed Borromean halo nuclei. (This name is derived from the heraldic symbol of the Borromeo family of Italy, which consists of three rings interlocked in such a way that if any one of the rings is removed, the other two separate.) The most carefully studied Borromean halo nuclei are ^{6}He and ^{11}Li, which have two weakly bound valence neutrons (107). In the case of ^{6}He, the core is a ^{4}He nucleus, which is also known as the α particle. The two-neutron separation energy for ^{6}He

is ∼1 MeV, which is small compared with the ∼28-MeV binding energy of the α particle. The $n\alpha$ system has no bound states, and the ^{6}He nucleus is therefore Borromean. There is, however, a strong P-wave resonance in the $J = 3/2$ channel of $n\alpha$ scattering, which is sometimes referred to as ^{5}He. This resonance is responsible for the binding of ^{6}He. Thus, ^{6}He can be interpreted as a bound state of an α particle and two neutrons, both of which are in $P_{3/2}$ configurations.

Because of the separation of scales in halo nuclei, they can be described by extensions of the pionless EFT. One can assume the core to be structureless and treat the nucleus as a few-body system of the core and the valence nucleons. Corrections from the structure of the core appear in higher orders and can be included in perturbation theory. Cluster models of halo nuclei then appear as LO approximations in this halo EFT. A new feature is the appearance of resonances as in the $n\alpha$ system, which leads to a more complicated singularity structure and renormalization compared with the few-nucleon system discussed above (108).

The first application of EFT methods to halo nuclei was carried out in References 108 and 109, in which the $n\alpha$ system (^{5}He) was considered. The authors found that for resonant P-wave interactions, both the scattering length and effective range have to be included nonperturbatively at LO. At threshold, however, only one combination of coupling constants is fine-tuned, and the EFT becomes perturbative. Because the $n\alpha$ interaction is resonant in the P-wave and not in the S-wave, the binding mechanism of ^{6}He is not the Efimov effect. However, this nucleus can serve as a laboratory in which to study the interplay of resonance structures in higher partial waves.

Three-body halo nuclei composed of a core and two valence neutrons are of particular interest due to these systems' potential to display the Efimov effect (3). Because the scattering length cannot be easily varied in halo nuclei, one looks for Efimov scaling between different states of the same nucleus. Such analyses assume that the halo ground state is an Efimov state.[2] They have previously been carried out in cluster models and the renormalized zero-range model (e.g., 110–112). A comprehensive study of S-wave halo nuclei in halo EFT was recently carried out (113). This work provided binding energy and structure calculations, including error estimates, for various halo nuclei. In a confirmation of earlier results by Fedorov et al. (110) and Amorim et al. (111), ^{20}C was found to be the only candidate nucleus for an excited Efimov state, assuming the ground state is also an Efimov state. This nucleus consists of a ^{18}C core with spin and parity quantum numbers $J^P = 0^+$ and two valence neutrons. The nucleus ^{19}C is expected to have a $\frac{1}{2}^+$ state near threshold, implying a shallow neutron-core bound state and therefore a large neutron-core scattering length. The value of the ^{19}C energy, however, is not known well enough to make a definite statement about the appearance of an excited state in ^{20}C. An excited state with a binding energy of ∼65 keV is marginally consistent with the current experimental information.

The matter form factors and radii of halo nuclei can also be calculated in the halo EFT (113, 114). As an example, we show the various one- and two-body matter density form factors $\mathcal{F}_c$, $\mathcal{F}_n$, $\mathcal{F}_{nc}$, and $\mathcal{F}_{nn}$ with LO error bands for the ground state of ^{20}C as a function of the momentum transfer k^2 (from Reference 113) in **Figure 11**. The theory breaks down for momentum transfers on the order of the pion mass squared ($k^2 \approx 0.5$ fm^{-2}).

From the slope of the matter form factors, one can extract the corresponding radii:

$$\mathcal{F}(k^2) = 1 - \frac{1}{6}k^2\langle r^2\rangle + \ldots. \qquad 44.$$

Information about these radii has been extracted from experiments for some halo nuclei based on intensity interferometry and Dalitz plots (115). Within the error estimates, the extracted values

[2]It is also possible that only the excited state is an Efimov state and that the ground state is more compact. This scenario cannot be ruled out, but it is also less predictive.

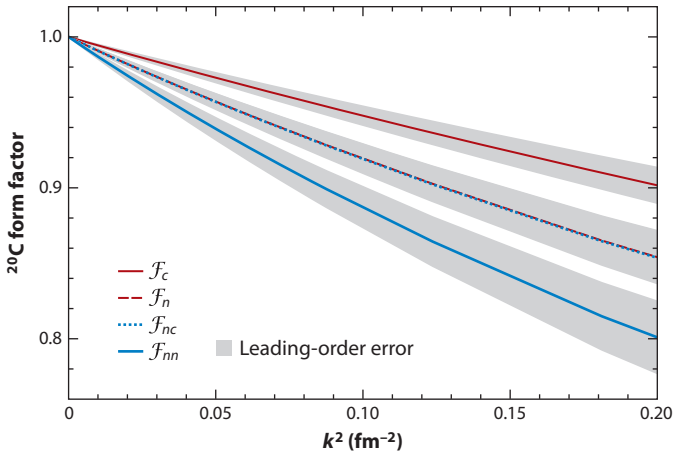

Figure 11

The one- and two-body matter density form factors $\mathcal{F}_c$, $\mathcal{F}_n$, $\mathcal{F}_{nc}$, and $\mathcal{F}_{nn}$ with leading-order error bands (*gray areas*) for the ground state of ^{20}C as a function of the momentum transfer k^2.

are in good agreement with the theoretical predictions from halo EFT (113). For the possible ^{20}C excited state, the halo EFT at LO predicts neutron-neutron and neutron-core radii of order 40 fm, whereas the ground-state radii are of order 2–3 fm. The theoretical errors are estimated to be of order 10%. Assuming a natural value for the effective range of the n-^{18}C interaction, $r_0 \approx 1/M_\pi$, NLO predictions for these radii have recently been obtained (116). The LO results were found to be stable under inclusion of the leading effective range corrections, and the typical errors could be reduced to approximately 1–2%.

Scattering observables offer a complementary window into Efimov physics in halo nuclei, and recent model studies have focused on this issue. Specifically, the trajectory of the possible ^{20}C excited state was extended into the scattering region to find a resonance in n-^{19}C scattering (117, 118). A detailed study of n-^{19}C scattering near an Efimov state was also carried out (119).

The simplest strange halo nucleus is the hypertriton, a three-body bound state composed of a proton, a neutron, and the Λ. The total binding energy is only approximately 2.4 MeV. The separation energy for the Λ, $E_\Lambda = 0.13$ MeV, is tiny compared with the binding energy of the deuteron, $B_d = 2.22$ MeV. The hypertriton can therefore also be considered a two-body halo nucleus. It has been studied in both two-body and three-body approaches (120–122). A study of the hypertriton in the halo EFT has been performed (123). The ΛN scattering lengths are not well known experimentally because the few scattering data are at relatively high energies. If the ΛN scattering lengths are large, the hypertriton is probably bound due to the Efimov effect. In this case, there would also be a correlation between the Λd scattering length $a_{\Lambda d}$ and the hypertriton binding energy B_t^Λ analog to the Phillips line in the neutron-deuteron system (121). In **Figure 12**, we show this Phillips line correlation for three values of the ΛN pole position γ_i (123). For small hypertriton energies B_t^Λ, the different Phillips lines coincide exactly (the physical hypertriton corresponds to $M\,B_t^\Lambda \approx 1.06\,\gamma_t^2$) and deviate from each other only at very large binding energies, at which the EFT breaks down. For all practical purposes, the Phillips line is therefore independent of γ_i. Whether the Efimov effect plays a role for the hypertriton is an open question. Most modern hyperon-nucleon potentials, however, favor a natural ΛN scattering length (54).

Another powerful method that can be used to investigate the Efimov effect in three-body halo nuclei at existing and future facilities with exotic beams (such as FAIR and FRIB) is Coulomb

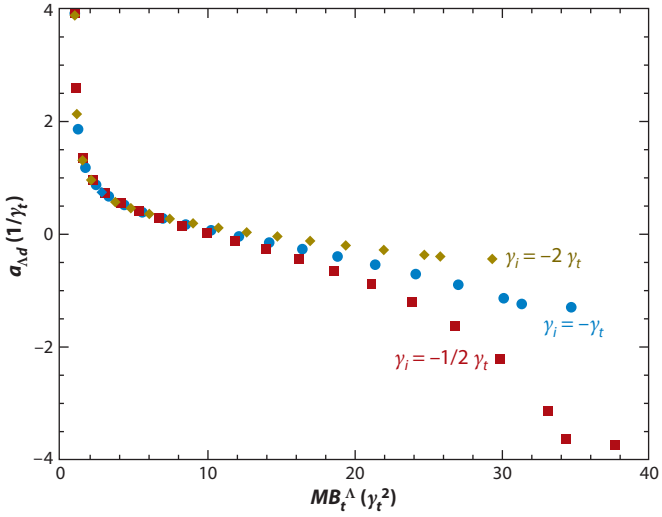

Figure 12

Phillips line in the hypertriton channel for different values of the ΛN pole position γ_i (all quantities are in units of the deuteron pole position $\gamma_t \approx 45$ MeV). Adapted from Reference 123 with permission.

excitation. In such experiments, a nuclear beam scatters off the Coulomb field of a heavy nucleus. Such processes can populate excited states of the projectile that subsequently decay, leading to its so-called Coulomb dissociation (124). The halo EFT offers a systematic framework for a full quantum-mechanical treatment and can be used to predict the signature of the Efimov effect in these reactions.

3.4. Three-Alpha System and Coulomb Interaction

The excited 0^+ state in ^{12}C is known as the Hoyle state. Its properties are important for stellar astrophysics because it determines the ratio of carbon to oxygen in stellar helium burning. Efimov suggested (3, 17) that the Hoyle state could be explained as a universal trimer of α particles. (For a more detailed discussion, see Reference 28.) In this case, the universal properties are modified by the long-range Coulomb interaction. The modified Efimov spectrum must be understood before any definite statement about the nature of the Hoyle state can be made.

Many recent studies have focused on the consistent inclusion of the Coulomb interaction in two-body halo nuclei such as the $p\alpha$ and $\alpha\alpha$ systems (125, 126). Specifically, the $\alpha\alpha$ system shows a surprising amount of fine-tuning between the strong and electromagnetic interactions. It can be understood in an expansion around the limit where, when the electromagnetic interactions are turned off, the ^{8}Be ground state is exactly at threshold and exhibits conformal invariance (126). In this scenario, the Hoyle state in ^{12}C would indeed appear as a remnant of an excited Efimov state. To better understand the modification of the Efimov spectrum and limit cycles by long-range interactions such as the Coulomb interaction, Hammer & Higa (127) investigated a one-dimensional inverse square potential supplemented with a Coulomb interaction. The results indicate that the counterterm required to renormalize the inverse square potential alone is sufficient to renormalize the full problem. However, the breaking of the discrete scale invariance through the Coulomb interaction leads to a modified bound-state spectrum. The shallow bound states are strongly influenced by the Coulomb interaction, whereas the deep bound states are dominated by the inverse

square potential. These results support the conjecture that the Hoyle state is an Efimov state of α particles, but a full calculation of the 3α system—including Coulomb in the halo EFT—is missing. Calculations with the fermionic molecular dynamics model and electron scattering data, however, support a pronounced α cluster structure of the Hoyle state (128).

4. APPLICATIONS IN PARTICLE PHYSICS

4.1. Hadronic Molecules

In recent years, many new and possibly exotic charmonium states have been observed at the B factories at SLAC, at KEK in Japan, and at the CESR collider at Cornell. These observations have revived the field of charmonium spectroscopy (129–131). Several of the new states exist very close to scattering thresholds and can be interpreted as hadronic molecules. If they are sufficiently shallow, one may ask whether there are any three-body hadronic molecules bound by the Efimov effect.

A particularly interesting example is the $X(3872)$, discovered by the Belle Collaboration (132) in $B^{\pm} \to K^{\pm}\pi^{+}\pi^{-}J/\psi$ decays and quickly confirmed by CDF (133), DØ (134), and BaBar (135). The state has likely quantum numbers $J^{PC} = 1^{++}$ and is very close to the $D^{*0}\bar{D}^{0}$ threshold. As a consequence, the $X(3872)$ has a resonant S-wave coupling to the $D^{*0}\bar{D}^{0}$ system. An extensive program provides predictions for its decay modes based on the assumption that it is a $D^{*0}\bar{D}^{0}$ molecule with even C-parity:

$$(D^{*0}\bar{D}^{0})_{+} \equiv \frac{1}{\sqrt{2}}\left(D^{*0}\bar{D}^{0} + D^{0}\bar{D}^{*0}\right). \qquad 45.$$

This assumption naturally explains several puzzling features, such as the apparently different mass in the $J/\psi\pi^{+}\pi^{-}$ and $D^{*0}\bar{D}^{0}$ decay channels and the isospin-violating decays (136, 137). A status report with references to the original literature can be found in Reference 138.

Use of the latest measurements in the $J/\psi\pi^{+}\pi^{-}$ channel show the mass of the $X(3872)$ (139) to be $m_X = (3{,}871.55 \pm 0.20)$ MeV, which corresponds to an energy relative to the $D^{*0}\bar{D}^{0}$ threshold of

$$E_X = (-0.26 \pm 0.41)\,\text{MeV}. \qquad 46.$$

The central value corresponds to a $(D^{*0}\bar{D}^{0})_{+}$ bound state with binding energy $B_X = 0.26$ MeV [but a virtual state cannot be excluded from the current data in the $J/\psi\pi^{+}\pi^{-}$ and $D^{*0}\bar{D}^{0}$ channels (140–142)]. The $X(3872)$ is also very narrow; its width is smaller than 2.3 MeV.

Because the $X(3872)$ is so close to the $D^{*0}\bar{D}^{0}$ threshold, it has universal low-energy properties that depend only on its binding energy (143). Close to threshold, the coupling to charged D mesons can be neglected because the $D^{*+}\bar{D}^{-}$ threshold is ~8 MeV higher in energy. Therefore, the properties of the $X(3872)$ can be described in a universal EFT with contact interactions only. Unfortunately, there is no Efimov effect in this system (143), so universal bound states of the X and D^{0} or D^{*0} mesons do not exist. The reason for this is that there are insufficient pairs with resonant interactions, as only the $D^{*0}\bar{D}^{0}$ and $D^{0}\bar{D}^{*0}$ interactions are resonant. However, it is possible to provide model-independent predictions for the scattering of D^{0} and D^{*0} mesons and their antiparticles off the $X(3872)$. This scattering process is determined to LO by the $D^{*0}\bar{D}^{0}$ and $D^{0}\bar{D}^{*0}$ interactions only.

The corresponding cross sections as a function of the center-of-mass momentum k (139) are shown in **Figure 13**. The difference between the contribution of S-waves ($L = 0$) and the full cross section (including all partial waves up to $L = 6$) is negligible for momenta below the bound-state pole momentum γ. Our results are given in units of the scattering length and may be scaled

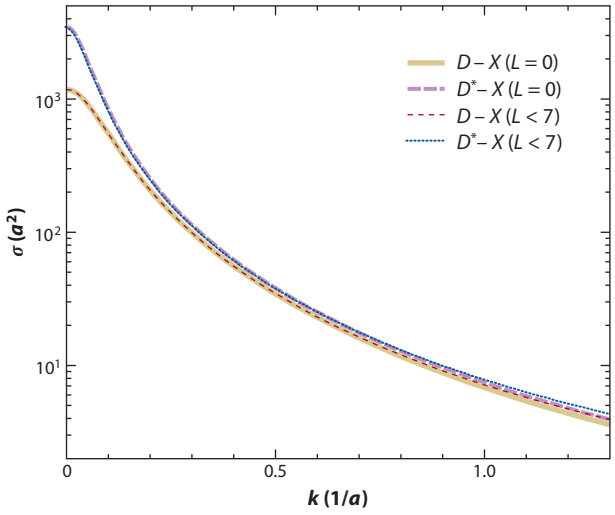

Figure 13

Total cross section for scattering of D^0 and D^{*0} mesons off the $X(3872)$ for S-waves ($L = 0$) and including higher partial waves with $L < 7$, in units of the scattering length a. The cross section is the same for the scattering of particles as it is for the scattering of antiparticles. Adapted from Reference 139 with permission.

to physical units once a is determined. At present, the error in the experimental value for E_X in Equation 43 implies a large error in the scattering length. Specifically, we obtain the range $\gamma = (0 \ldots 36)$ MeV for the pole momentum and the range $a = (5.5 \ldots \infty)$ fm for the scattering length with central values $\gamma = 22$ MeV and $a = 8.8$ fm. Using the central value of the scattering length, we obtain for the scale factor $a^2 = 0.78$ b. This factor can become infinite if the $X(3872)$ is directly at threshold, whereas the lower bound from the error in E_X would give a value of 0.3 b. Even in this case, the total cross section at threshold would be of the order of 300 b for D^0X scattering and 1,000 b for $D^{0*}X$ scattering. It may be possible to extract the scattering within the final-state interactions of B_c decays and/or other LHC events. Observation of enhanced final-state interactions would provide an independent confirmation of the nature of the $X(3872)$.

There may also be hadronic three-body molecules that are bound due to the Efimov effect, but currently no strong candidate states are known. This situation will be improved by new experiments at facilities such as FAIR and Belle II, which have a dedicated program to study exotic charmonium states.

5. SUMMARY AND OUTLOOK

Any few-body system with short-range interactions that has a two-body scattering length larger than the range of the underlying interaction displays universal properties and Efimov physics. This statement is independent of the typical length scale of the system, and atomic, nuclear, and particle physics can provide examples of universality. Although much progress has recently been made in experiments with ultracold atoms, the concept of Efimov physics was originally devised for the few-nucleon problem. As we have shown, it can serve as a starting point for a description of very low energy nuclear phenomena in an expansion around the unitary limit.

In this review, we have discussed the manifestation of Efimov physics with a strong emphasis on nuclear and particle physics. There are a number of such systems that display low-energy universality associated with Efimov physics. The most important example from nuclear physics is the

triton. The nucleon-nucleon scattering length is large compared with the range of the internuclear interaction. Phase shift–equivalent nucleon-nucleon potentials therefore necessarily give results for the triton binding energy and neutron-deuteron scattering length that are correlated and lie on the Phillips line. The implications of universality on the four-nucleon system have also been explored. The Tjon line, a correlation between three-nucleon and four-nucleon binding energies, is a result of the large two-nucleon scattering length.

Halo nuclei could provide a further example of few-body universality. Specifically, two-neutron halos such as ^{20}C could display Efimov physics in the form of an excited three-body state due to the large core-neutron scattering length. Although initial studies of bound-state observables have become available, scattering calculations represent an exciting opportunity for future applications of the EFT approach. So-called $p - t$ reactions, in which a triton is formed in a collision of a proton and a two-neutron halo, will provide an important benchmark.

Several new charmonium states have recently been discovered close to scattering thresholds and can be interpreted as hadronic molecules. If they are sufficiently shallow, they have universal properties associated with large scattering length physics. The best-known example is the $X(3872)$, which may be interpreted as a $D^{*0}\bar{D}^0$ molecule with even C-parity. There may also be three-body hadronic molecules bound by the Efimov effect, but currently no strong candidates are known.

The separation of scales between scattering length and range facilitates the application of an EFT that reproduces at LO the results obtained by Efimov and is known as pionless EFT. Within this framework, corrections to the zero-range limit can be calculated systematically in a small parameter expansion in powers of $k\ell$ and ℓ/a. The number of few-body calculations that include higher-order corrections is growing. As a consequence, the expansion around the unitary limit provides a useful starting point for a controlled description of very low energy phenomena in nuclear and particle physics. The intricate consequences of Efimov physics are explicit in this framework, and universal correlations between observables arise naturally. Moreover, this theory is an ideal tool with which to unravel universal properties and establish connections between different fields of physics.

The constituents of nuclear few-body systems can have charge, unlike the neutral atoms used in experiments with ultracold gases. Electroweak observables thus provide additional information about few-body universality. However, they are also of interest by themselves, and pionless EFT guarantees a consistent framework for the calculation of observables with the minimal number of parameters because it is straightforward to consider external currents in any EFT. The first calculations for observables such as form factors and capture rates have been performed, but many more remain to be calculated. Of very great interest in this context are thermal capture rates in the four-nucleon sector that are relevant to big bang nucleosynthesis.

DISCLOSURE STATEMENT

The authors are not aware of any affiliations, memberships, funding, or financial holdings that might be perceived as affecting the objectivity of this review.

ACKNOWLEDGMENTS

We thank Eric Braaten and Vitaly Efimov for discussions. Our research was supported by the National Science Foundation under grant number PHY-0653312, by the UNEDF SciDAC Collaboration under U.S. Department of Energy grant numbers DE-FC02-07ER41457 and DE-FG02-00ER41132, by the Deutsche Forschungsgemeinschaft through SFB/TR16, and by

the Bundesministerium für Bildung und Forschung under contract numbers 06BN411 and 06BN9006.

LITERATURE CITED

1. Braaten E, Hammer HW. *Phys. Rep.* 428:259 (2006)
2. Platter L. *Few Body Syst.* 46:139 (2009)
3. Efimov V. *Phys. Lett.* B33:563 (1970)
4. Schöllkopf W, Toennies J. *Science* 266:1345 (1994)
5. Kraemer T, et al. *Nature* 440:315 (2006)
6. Braaten E, Hammer HW. *Ann. Phys.* 322:120 (2007)
7. Thomas L. *Phys. Rev.* 47:903 (1935)
8. Skorniakov GV, Ter-Martirosian KA. *Sov. Phys. JETP* 4:648 (1957)
9. Danilov G. *Sov. Phys. JETP* 13:349 (1961)
10. Faddeev LD, Minlos RA. *Sov. Phys. JETP* 14:1315 (1962)
11. Minlos RA, Faddeev LD. *Sov. Phys. Dokl.* 6:1072 (1962)
12. Danilov G, Lebedev V. *Sov. Phys. JETP* 17:1015 (1963)
13. Amado RD, Noble JV. *Phys. Lett.* B35:25 (1971)
14. Amado RD, Noble JV. *Phys. Rev. D* 5:1992 (1972)
15. Adhikari SK, et al. *Phys. Rev. A* 37:3666 (1988)
16. Albeverio S, Hegh-Krohn R, Wu TT. *Phys. Lett.* A83:105 (1981)
17. Efimov V. *Sov. J. Nucl. Phys.* 12:589 (1971)
18. Efimov V. *Sov. J. Nucl. Phys.* 29:546 (1979)
19. Efimov V. *Nucl. Phys. A* 362:45 (1981)
20. Efimov V. *Phys. Rev. C* 44:2303 (1991)
21. Bedaque PF, van Kolck U. *Phys. Lett.* B428:221 (1998)
22. Bedaque PF, Hammer HW, van Kolck U. *Phys. Rev. C* 58:R641 (1998)
23. Bedaque PF, Hammer HW, van Kolck U. *Nucl. Phys. A* 676:357 (2000)
24. Wigner E. *Phys. Rev.* 51:106 (1937)
25. Mehen T, Stewart IW, Wise MB. *Phys. Rev. Lett.* 83:931 (1999)
26. Nielsen E, Fedorov D, Jensen A, Garrido E. *Phys. Rep.* 347:373 (2001)
27. Jensen AS, Riisager K, Fedorov DV, Garrido E. *Rev. Mod. Phys.* 76:215 (2004)
28. Efimov V. *Comm. Nucl. Part. Phys.* 19:271 (1990)
29. Braaten E, Phillips D. *Phys. Rev. A* 70:052111 (2004)
30. Bedaque PF, Hammer HW, van Kolck U. *Phys. Rev. Lett.* 82:463 (1999)
31. Platter L, Ji C, Phillips DR. *Phys. Rev. A* 79:022702 (2009)
32. Phillips A. *Nucl. Phys. A* 107:209 (1968)
33. Platter L, Hammer HW, Meissner U-G. *Phys. Rev. A* 70:052101 (2004)
34. Hammer HW, Platter L. *Eur. Phys. J. A* 32:113 (2007)
35. von Stecher J, D'Incao J, Greene C. *Nat. Phys.* 5:417 (2009)
36. Ferlaino F, et al. *Phys. Rev. Lett.* 102:140401 (2009)
37. von Stecher J. *J. Phys. B* 43:101002 (2010)
38. Knoop S, et al. *Nat. Phys.* 5:227 (2009)
39. Helfrich K, Hammer HW. *Europhys. Lett.* 86:53003 (2009)
40. Zaccanti M, et al. *Nat. Phys.* 5:586 (2009)
41. Barontini G, et al. *Phys. Rev. Lett.* 103:043201 (2009)
42. Gross N, Shotan Z, Kokkelmans S, Khaykovich L. *Phys. Rev. Lett.* 103:163202 (2009)
43. Pollack SE, Dries D, Hulet RG. *Science* 326:1683 (2009)
44. Bartenstein M, et al. *Phys. Rev. Lett.* 94:103201 (2005)
45. Ottenstein TB, et al. *Phys. Rev. Lett.* 101:203202 (2008)
46. Huckans JH, et al. *Phys. Rev. Lett.* 102:165302 (2009)
47. Braaten E, Hammer HW, Kang D, Platter L. *Phys. Rev. Lett.* 103:073202 (2009)

48. Naidon P, Ueda M. *Phys. Rev. Lett.* 103:073203 (2009)
49. Floerchinger S, Schmidt R, Wetterich C. *Phys. Rev. A* 79:053633 (2009)
50. Williams JR, et al. *Phys. Rev. Lett.* 103:130404 (2009)
51. Lompe T, et al. arXiv:1003.0600 [cond-mat] (2010)
52. Beane SR, et al. arXiv:nucl-th/0008064 (2000)
53. Bedaque PF, van Kolck U. *Annu. Rev. Nucl. Part. Sci.* 52:339 (2002)
54. Epelbaum E, Hammer HW, Meissner U-G. *Rev. Mod. Phys.* 81:1773 (2009)
55. Mohr RF, et al. *Ann. Phys.* 321:225 (2006)
56. Braaten E, Hammer HW. *Phys. Rev. Lett.* 91:102002 (2003)
57. Epelbaum E. *Prog. Part. Nucl. Phys.* 57:654 (2006)
58. Kaplan DB, Savage MJ, Wise MB. *Nucl. Phys. B* 534:329 (1998)
59. Birse MC, McGovern JA, Richardson KG. *Phys. Lett.* B464:169 (1999)
60. Kaplan DB. *Nucl. Phys. B* 494:471 (1997)
61. Phillips DR, Rupak G, Savage MJ. *Phys. Lett.* B473:209 (2000)
62. Bedaque PF, Hammer HW, van Kolck U. *Nucl. Phys. A* 646:444 (1999)
63. Kharchenko VF. *Sov. J. Nucl. Phys.* 16:173 (1973)
64. Hammer HW, Mehen T. *Nucl. Phys. A* 690:535 (2001)
65. Afnan IR, Phillips DR. *Phys. Rev. C* 69:034010 (2004)
66. Bedaque PF, Rupak G, Griesshammer HW, Hammer HW. *Nucl. Phys. A* 714:589 (2003)
67. Griesshammer HW. *Nucl. Phys. A* 744:192 (2004)
68. Platter L, Phillips DR. *Few Body Syst.* 40:35 (2006)
69. Platter L. *Phys. Rev. C* 74:037001 (2006)
70. Gabbiani F, Bedaque PF, Griesshammer HW. *Nucl. Phys. A* 675:601 (2000)
71. Griesshammer HW. *Nucl. Phys. A* 760:110 (2005)
72. Wilson KG. *Rev. Mod. Phys.* 55:583 (1983)
73. Barford T, Birse MC. *J. Phys. A* 38:697 (2005)
74. Birse MC. *Phys. Rev. C* 77:047001 (2008)
75. Ando S-I, Birse MC. *Phys. Rev. C* 78:024004 (2008)
76. Platter L, Hammer HW. *Nucl. Phys. A* 766:132 (2006)
77. Sadeghi H, Bayegan S. *Nucl. Phys. A* 753:291 (2005)
78. Sadeghi H, Bayegan S, Griesshammer HW. *Phys. Lett.* B643:263 (2006)
79. Sadeghi H. *Phys. Rev. C* 75:044002 (2007)
80. Sadeghi H. arXiv:0908.2052 [nucl-th] (2009)
81. Sadeghi H, Bayegan S. *Few Body Syst.* 47:167 (2010)
82. Platter L, Hammer HW, Meissner U-G. *Phys. Lett.* B607:254 (2005)
83. Nogga A, Kamada H, Gloeckle W. *Phys. Rev. Lett.* 85:944 (2000)
84. Epelbaum E, et al. *Phys. Rev. Lett.* 86:4787 (2001)
85. Epelbaum E, et al. *Phys. Rev. C* 66:064001 (2002)
86. Nogga A, Bogner SK, Schwenk A. *Phys. Rev. C* 70:061002 (2004)
87. Kirscher J, Griesshammer HW, Shukla D, Hofmann HM. *Eur. Phys. J. A* 44:239 (2010)
88. Kirscher J, Griesshammer HW, Shukla D, Hofmann HM. arXiv:0909.5606 [nucl-th] (2009)
89. Stetcu I, Barrett BR, van Kolck U. *Phys. Lett.* B653:358 (2007)
90. Stetcu I, Barrett BR, van Kolck U, Vary JP. *Phys. Rev. A* 76:063613 (2007)
91. Stetcu I, Rotureau J, Barrett BR, van Kolck U. *J. Phys. G* 37:064033 (2010)
92. Beane SR, Savage MJ. *Nucl. Phys. A* 717:91 (2003)
93. Epelbaum E, Meissner U-G, Gloeckle W. *Nucl. Phys. A* 714:535 (2003)
94. Beane SR, Bedaque PF, Savage MJ, van Kolck U. *Nucl. Phys. A* 700:377 (2002)
95. Epelbaum E, Meissner U-G, Gloeckle W, Elster C. *Phys. Rev. C* 65:044001 (2002)
96. Fettes N. *Pion-nucleon physics in chiral perturbation theory*. Ph.D. thesis. Univ. Bonn. 273 pp. (2000)
97. Fukugita M, et al. *Phys. Rev. Lett.* 73:2176 (1994)
98. Fukugita M, et al. *Phys. Rev. D* 52:3003 (1995)
99. Beane SR, Bedaque PF, Orginos K, Savage MJ. *Phys. Rev. Lett.* 97:012001 (2006)
100. Epelbaum E, Hammer HW, Meissner U-G, Nogga A. *Eur. Phys. J. C* 48:169 (2006)

101. Hammer HW, Phillips DR, Platter L. *Eur. Phys. J. A* 32:335 (2007)
102. Wilson KG. *Nucl. Phys. Proc. Suppl.* 140:3 (2005)
103. Beane SR, et al. *Phys. Rev. D* 80:074501 (2009)
104. Beane SR, Orginos K, Savage MJ. *Int. J. Mod. Phys.* E17:1157 (2008)
105. Kreuzer S, Hammer HW. *Phys. Lett.* B673:260 (2009)
106. Kreuzer S, Hammer HW. *Eur. Phys. J. A* 43:229 (2010)
107. Zhukov MV, et al. *Phys. Rep.* 231:151 (1993)
108. Bertulani CA, Hammer HW, van Kolck U. *Nucl. Phys. A* 712:37 (2002)
109. Bedaque PF, Hammer HW, van Kolck U. *Phys. Lett.* B569:159 (2003)
110. Federov DV, Jensen AS, Riisager K. *Phys. Rev. Lett.* 73:2817 (1994)
111. Amorim AEA, Frederico T, Tomio L. *Phys. Rev. C* 56:R2378 (1997)
112. Mazumdar I, Arora V, Bhasin VS. *Phys. Rev. C* 61:051303 (2000)
113. Canham DL, Hammer HW. *Eur. Phys. J. A* 37:367 (2008)
114. Yamashita MT, Tomio L, Frederico T. *Nucl. Phys. A* 735:40 (2004)
115. Marques FM, et al. *Phys. Rev. C* 64:061301 (2001)
116. Canham DL, Hammer HW. *Nucl. Phys. A* 836:275 (2010)
117. Yamashita MT, Frederico T, Tomio L. *Phys. Lett.* B660:339 (2008)
118. Mazumdar I, Rau ARP, Bhasin VS. *Phys. Rev. Lett.* 97:062503 (2006)
119. Yamashita MT, Frederico T, Tomio L. *Phys. Lett.* B670:49 (2008)
120. Cobis A, Jensen AS, Fedorov DV. *J. Phys. G* 23:401 (1997)
121. Fedorov DV, Jensen AS. *Nucl. Phys. A* 697:783 (2002)
122. Congleton JG. *J. Phys. G* 18:339 (1992)
123. Hammer HW. *Nucl. Phys. A* 705:173 (2002)
124. Bertulani CA, Baur G. *Phys. Rep.* 163:299 (1988)
125. Higa R. *Mod. Phys. Lett. A* 24:915 (2009)
126. Higa R, Hammer HW, van Kolck U. *Nucl. Phys. A* 809:171 (2008)
127. Hammer HW, Higa R. *Eur. Phys. J. A* 37:193 (2008)
128. Chernykh M, et al. *Phys. Rev. Lett.* 98:032501 (2007)
129. Eichten E, Godfrey S, Mahlke H, Rosner JL. *Rev. Mod. Phys.* 80:1161 (2008)
130. Voloshin MB. *Prog. Part. Nucl. Phys.* 61:455 (2008)
131. Godfrey S, Olsen SL. *Annu. Rev. Nucl. Part. Sci.* 58:51 (2008)
132. Choi SK, et al. (Belle Collab.) *Phys. Rev. Lett.* 91:262001 (2003)
133. Acosta DE, et al. (CDF II Collab.) *Phys. Rev. Lett.* 93:072001 (2004)
134. Abazov VM, et al. (DØ Collab.) *Phys. Rev. Lett.* 93:162002 (2004)
135. Aubert B, et al. (BaBar Collab.) *Phys. Rev. D* 71:071103 (2005)
136. Braaten E, Lu M. *Phys. Rev. D* 76:094028 (2007)
137. Braaten E, Lu M. *Phys. Rev. D* 77:014029 (2008)
138. Braaten E. arXiv:0808.2948 [hep-ph] (2008)
139. Canham DL, Hammer HW, Springer RP. *Phys. Rev. D* 80:014009 (2009)
140. Bugg DV. *Phys. Lett.* B598:8 (2004)
141. Hanhart C, Kalashnikova YS, Kudryavtsev AE, Nefediev AV. *Phys. Rev. D* 76:034007 (2007)
142. Voloshin MB. *Phys. Rev. D* 76:014007 (2007)
143. Braaten E, Kusunoki M. *Phys. Rev. D* 69:074005 (2004)

Annual Review of Nuclear and Particle Science

Volume 60, 2010

Contents

Indexes

Errata

An online log of corrections to *Annual Review of Nuclear and Particle Science* articles may be found at http://nucl.annualreviews.org/errata.shtml